### Title

Precise Temporal Disaggregation Preserving Marginals and Correlations (DiPMaC) for Stationary and Nonstationary Processes




### Journal

Water Resources Research, 54(10)

### ISSN

0043-1397



### Authors

Papalexiou, Simon Michael
Markonis, Yannis
Lombardo, Federico
et al.



### Publication Date

2018-10-01

### DOI

10.1029/2018wr022726

Peer reviewed

Water Resources Research

RESEARCH ARTICLE
10.1029/2018WR022726

**Key Points:**
- Novel model enables disaggregation at any time scale by reproducing the marginal distribution and the correlation structure of the fine-scale process
- The model involves optimized algorithmic efficiency based on a novel Bernoulli-trials framework
- The model is applicable to both stationary and nonstationary processes

**Supporting Information:**
- Supporting Information S1

**Correspondence to:**
S. M. Papalexiou,
sm.papalexiou@usask.ca

**Citation:**
Papalexiou, S. M., Markonis, Y., Lombardo, F., AghaKouchak, A., & Foufoula-Georgiou, E. (2018). Precise temporal Disaggregation Preserving Marginals and Correlations (DiPMaC) for stationary and nonstationary processes. *Water Resources Research*, *54*, 7435–7458. https://doi.org/10.1029/2018WR022726

Received 6 FEB 2018
Accepted 28 AUG 2018
Accepted article online 4 SEP 2018
Published online 8 OCT 2018



# Precise Temporal Disaggregation Preserving Marginals and Correlations (DiPMaC) for Stationary and Nonstationary Processes

**Simon Michael Papalexiou[1,2,3], Yannis Markonis[4], Federico Lombardo[5], Amir AghaKouchak[3], and Efi Foufoula-Georgiou[3]**

[1]Department of Civil, Geological and Environmental Engineering, University of Saskatchewan, Saskatoon, Saskatchewan, Canada, [2]Global Institute for Water Security, Saskatoon, Saskatchewan, Canada, [3]Department of Civil and Environmental Engineering, University of California, Irvine, CA, USA, [4]Faculty of Environmental Sciences, Czech University of Life Sciences Prague, Prague, Czech Republic, [5]Dipartimento di Ingegneria Civile, Edile e Ambientale, Sapienza Università di Roma, Rome, Italy

**Abstract** Hydroclimatic variables such as precipitation and temperature are often measured or simulated by climate models at coarser spatiotemporal scales than those needed for operational purposes. This has motivated more than half a century of research in developing disaggregation methods that break down coarse-scale time series into finer scales, with two primary objectives: (a) reproducing the statistical properties of the fine-scale process and (b) preserving the original coarse-scale data. Existing methods either preserve a limited number of statistical moments at the fine scale, which is often insufficient and can lead to an unrepresentative approximation of the actual marginal distribution, or are based on a limited number of a priori distributional assumptions, for example, lognormal. Additionally, they are not able to account for potential nonstationarity in the underlying fine-scale process. Here we introduce a novel disaggregation method, named Disaggregation Preserving Marginals and Correlations (DiPMaC), that is able to disaggregate a coarse-scale time series to any finer scale, while reproducing the probability distribution and the linear correlation structure of the fine-scale process. DiPMaC is also generalized for arbitrary nonstationary scenarios to reproduce time varying marginals. Additionally, we introduce a computationally efficient algorithm, based on Bernoulli trials, to optimize the disaggregation procedure and guarantee preservation of the coarse-scale values. We focus on temporal disaggregation and demonstrate the method by disaggregating monthly precipitation to hourly, and time series with trends (e.g., climate model projections), while we show its potential to disaggregate based on general nonstationary scenarios. The example applications demonstrate the performance and robustness of DiPMaC.

## 1. Half Century of Disaggregation

Half a century has passed since the first disaggregation attempt by Harms and Campbell (1967) for simulation of the river Nile flow. Their early approach was soon followed by the milestone papers of Valencia and Schaake (1972, 1973), which presented a general case for the model proposed by Matalas (1967) as a complete methodological scheme, the so-called disaggregation model. The whole framework was based upon breaking down a sequence of coarser time scale (e.g., monthly) values into a sequence of finer time scale (e.g., daily) values, generating synthetic time series that reproduce the statistical characteristics of the observed records (or model outputs), both at the time scale of simulation and across coarser scales. Several modifications were proposed in the following years; for instance, Mejia and Rousselle (1976) included linkages with consecutive periods at the different levels of aggregation, while the scheme was also used in a multivariate application that preserved cross-correlation between different time series (Tao & Delleur, 1976). Loucks et al. (1981) suggested implementing disaggregation in stages by first disaggregating the variables into individual sites, and then individual series were further disaggregated into their seasonal values. Stedinger and Vogel (1984) used a first-order autoregressive model to introduce short-term linear dependence and reproduce more successfully the variance and covariance properties of the disaggregated time series, but they also showed that the structure of these disaggregation models places severe constraints on the reproduction of the exact historical serial correlations at the scale of simulation.

Furthermore, these methods did not preserve higher order moments in time series with non-Gaussian marginal distributions or the actual marginal itself. Therefore, Valencia and Schaake (1973) underlined the necessity to use some suitable transformation of the time series into Gaussian, before applying a disaggregation scheme. Typical transformations are the Box-Cox transform (Box & Cox, 1964; Tao & Delleur, 1976) and the logarithmic transform (e.g., Salas, 1980). At the same time efforts were undertaken to explicitly preserve the skewness of the seasonal distributions of streamflow (Hoshi & Burges, 1979; Srikanthan, 1978; Todini, 1980), which, however, did not maintain the additive property of the original aggregation scheme (Salas et al., 1985).

Multisite, multiseason disaggregation models can have a large number of parameters because of the many cross correlations that they attempt to reproduce (Grygier & Stedinger, 1988). This led to developing staged disaggregation procedures that disaggregate annual flows at one or more sites to seasonal flows in two or more steps, and to the condensed disaggregation models, which reduce the number of required parameters by explicitly modeling only a selected set of correlations among the seasonal flows (Grygier & Stedinger, 1988; Lane, 1979; Lane & Frevert, 1988; Oliveira et al., 1988; Pereira et al., 1984; Salas, 1980; Stedinger et al., 1985; Stedinger & Vogel, 1984).

In the same period, global circulation models (GCMs) started to offer the first simulations of the global climate and soon the question was risen (see Maraun & Widmann, 2018, for a historical review) whether they can be used to describe climatic features at finer scales and how this could be achieved (Kim et al., 1984). To answer this question many different directions were followed, namely, classified as empirical, semiempirical, and model-based (Giorgi & Mearns, 1991). The most popular semiempirical schemes were based on regression from the coarser to the finer scales (Hay et al., 1991; Karl et al., 1990; Kim et al., 1984; von Storch et al., 1993; Wigley et al., 1990). These schemes use other atmospheric circulation predictor variables at the regional scale, based on the assumptions that relationships can be established between atmospheric processes occurring at different spatiotemporal scales and that these relationships remain constant in time (Perica & Foufoula-Georgiou, 1996; Wilby & Wigley, 1997). Disaggregation methods are another important manifestation of wider efforts to scale down GCM outputs for impact studies (e.g., downscaling of climate change scenarios for hydrological applications).

We note that although both disaggregation and downscaling models refer to transferring information from coarser to finer scales, the term "downscaling" has been used mainly in relation to climatic models, for example, spatial downscaling of GCMs, while it is more general as it includes not only statistical approaches like analog methods (e.g., Zorita & von Storch, 1999) but also dynamical methods which are based on physical meteorological processes (e.g., Wood et al., 2004; Xue et al., 2014). On the other hand, the term "disaggregation" has mainly been used in the hydrological literature and refers to statistical methods that most commonly have been applied in the temporal disaggregation of rainfall (e.g., Glasbey et al., 1995). Additionally, most disaggregation schemes require to produce a finer scale time series that adds up to the given coarse-scale total (Lombardo et al., 2012). In these parallel paths between hydrological and climatological studies, it soon became apparent that precipitation is probably the most challenging process to efficiently disaggregate/downscale (e.g., Wilby & Wigley, 1997).

One of the most promising approaches to disaggregate precipitation has been based on the Bartlett-Lewis rectangular pulse model (Rodriguez-Iturbe et al., 1987), as applied by Glasbey et al. (1995), which had led to many subsequent models (e.g., Connolly et al., 1998; Cowpertwait et al., 1996; Kossieris et al., 2018; Koutsoyiannis & Onof, 2001). Other similar methods disaggregate daily precipitation into individual storms (Hershenhorn & Woolhiser, 1987), or used a geometric distribution to model rainfall occurrence and a beta distribution to simulate dimensionless accumulated hourly amounts aiming to preserve the first three moments (Kottegoda et al., 2003). Note also that using linear models to preserve moments results in nonrealistic correlation structures (Tsoukalas et al., 2018). Multifractal simulation schemes based on multiplicative cascade processes (e.g., Gupta & Waymire, 1990; Lovejoy & Schertzer, 1990) are another common methodological approach to perform disaggregation of precipitation records (Deidda, 2000; Molnar & Burlando, 2005; Olsson, 1998; Perica & Foufoula-Georgiou, 1996; Serinaldi, 2010; Venugopal et al., 1999), while a theoretically consistent stochastic cascade focusing on temporal disaggregation of intermittent rainfall reproducing also long-term persistence with Lognormal marginals was presented by Lombardo et al. (2017). Interestingly, the study of Perica and Foufoula-Georgiou (1996) on spatial disaggregation of rainfall using the convective

available potential energy as a predictor was one of the first cases where hydrological and climatological methodologies converged, mainly because climate studies were also searching for the most suitable predictors for precipitation downscaling, as highlighted by Wilby and Wigley (2000) and references therein.

During the last decade the strength of the application of statistical methods to climate model simulations has been acknowledged (see, e.g., Maraun et al., 2010, and references therein). Notable references include the generalized linear and additive models (e.g., Dobson & Barnett, 2008), chaotic disaggregation models (Sivakumar et al., 2001), support vector machines (Tripathi et al., 2006), vector generalized linear/additive models (Yee & Stephenson, 2007), quantile mapping (Maraun, 2013), and nonparametric techniques (Prairie et al., 2007) based on bootstrap k-nearest neighbor resampling algorithms (Lall & Sharma, 1996). Data-driven modeling techniques based on bootstrap have been widely applied (Lu & Qin, 2014; Nowak et al., 2010; Portela & Silva, 2016; Pui et al., 2012; Westra, Mehrotra et al., 2012), although they exhibit potential limitations, such as the lack of extrapolation beyond the observed records (Beersma & Buishand, 2003) or a poor exploration (and reproduction) of the state space due to insufficient sample sizes (especially in the case of stratified bootstrap). However, while the former shortcoming can be corrected by using for instance information from nearby locations (e.g., Westra, Mehrotra et al., 2012), the latter can be overcome only if longer sequences of records are made available. Pui et al. (2012) provided a comparison of some of the above disaggregation methods (i.e., random multiplicative cascades, point processes, and resampling).

Fifty years after the first disaggregation methodological attempts, both hydrological and climatic communities have a broad range of different methodologies to transform time series into finer scales. Current disaggregation methods in hydrology typically provide insufficient approximations of the fine-scale process or ad hoc solutions. On the other hand, GCMs seldom capture climatic variability at all temporal and/or spatial scales (see, e.g., Gehne et al., 2016; Karl et al., 1990; Kundzewicz & Stakhiv, 2010; Svoboda et al., 2017). The biggest discrepancies among GCM model outputs seem to appear at finer spatiotemporal scales relevant to hydrologic applications (Hostetler, 1994). Our methodology aims to provide a potential solution to this issue by presenting a precise disaggregation at any timescale under stationary and nonstationary conditions. The method goes beyond attempting to preserve a limited number of statistical moments and correlations, which leads to unreliable approximations of the actual probability distribution and of the correlation structure. In contrast, it enables, using a unified stochastic modeling scheme (Papalexiou, 2018), to disaggregate coarse-scale time series at any finer time scale by preserving the actual marginal distribution and the actual correlation structure of the fine-scale process.

## 2. Making Disaggregation Precise

### 2.1. Definition of Disaggregation

Hydroclimatic processes at all subannual timescales are commonly modeled by cyclostationary stochastic processes (if other forms of nonstationarity are not assumed) given that their statistical and stochastic properties (partly or all of them) vary cyclically over the year. Thus, a cyclostationary process can be decomposed into a set of stationary processes each one of which is valid for a specific subperiod of the year, for example, a month, a day, or even an hour. Let $\{X_s(t) | \, t \in T, s = 1, \ldots, N\}$ be a cyclostationary process with $T$ denoting an indexed set and $s$ a cyclically varying index over $t$ indicating the $s$th stationary process (hereafter $\{X_s(t)\}$ denotes the stationary process at subperiod $s$). For example, a process at daily scale, presumed stationary at each month, will have $N = 12$ stationary processes with $\{X_1(t)\}$ describing the first 31 days of the year, $\{X_2(t)\}$ the next 28 or 29 days, and so on. Also, each $\{X_s(t)\}$ process is described by a marginal distribution function $F_{X_s}(x)$ (continuous or mixed type in the case of intermittent processes) and an autocorrelation structure (ACS) $\rho_{X_s}(\tau)$.

Let us assume a cyclostationary process at timescale $k_0$ (basic or target timescale) decomposed into $N$ stationary processes, with period $n_p$, that is, $X_s(t) = X_s(t + n_p)$ and with the $s$th process valid for a subperiod of $n_s$ values, thus, $n_p = \sum_{s=1}^{N} n_s$. Clearly, $n_p$ depends on the $k_0$ units and the period, while $n_s$ on the subperiod where the $s$th process is valid, for example, in an annual cycle with presumed monthly stationarity and with $k_0 = 1$ hour, $n_p = 24 \times 365$ (or 366 for leap years) and $n_s = 24 \times D_s$ where $D_s$ is the number of days of the $s$th month. We denote the nonoverlapping aggregated (or averaged) process at timescale $k = m \times k_0$ ($m$ is any positive integer larger than 1) as $\{X_s^{(k)}(j)\}$ and we define its $j$th aggregated random variable (r.v.) as

$$X_s^{(k)}(j) \coloneqq \sum_{t=(j-1)k+1}^{jk} X_s(t) \tag{1}$$

where $X_s(t) \coloneqq X_s^{(k_0)}(t)$; for notational simplicity we omit the $k_0$ indicator hereafter. Let

$$\left\{x_s^{(k)}(j)\right\} \coloneqq \left\{x_1^{(k)}(1), \ldots, x_s^{(k)}(j), \ldots, x_N^{(k)}\left(n_p/k\right), \ldots\right\} \tag{2}$$

be an observed time series of the process $\{X_s^{(k)}(j)\}$ at the coarse time scale $k$, and let

$$\boldsymbol{x}_s(j) \coloneqq \{x_s(t)\}_{t=(j-1)k+1}^{jk} \tag{3}$$

be a random block of $k$ values ($k$-block hereafter) at a target fine time scale $k_0$. Disaggregation aims to find a time series

$$\{x_s(t)\} \coloneqq \left\{\boldsymbol{x}_1(1), \ldots, \boldsymbol{x}_s(j), \ldots, \boldsymbol{x}_N\left(n_p/k\right), \ldots\right\} \tag{4}$$

which, ideally, reproduces precisely the stochastic properties of the fine-scale process $\{X_s(t)\}$ by preserving the actual marginal distributions and the ACSs in all subperiods $s$, and additionally, the $k$-blocks are constrained by $\sum_{t=(j-1)k+1}^{jk} x_s(t) = x_s^{(k)}(j)$.

The disaggregation scheme we propose comprises two parts: (a) the fit and use of a precise stochastic model (the disaggregation kernel hereafter) capable of reproducing desired marginal distributions and linear correlation structures at the target timescale $k_0$ (Papalexiou, 2018) and (b) an optimization part, based on Bernoulli trials, which uses generated random $k$-blocks from the kernels in order to find those that match the imposed constraints, that is, make the disaggregated time series consistent with the coarse-scale totals (or mean values alternatively). Consequently, this framework is one-step method disaggregating the coarse-scale values directly to the target time scale values avoiding thus cascading techniques. We term this method DiPMaC (Disaggregation Preserving Marginals and Correlations).

We stress that for notational clarity, in the subsequent sections, whenever possible and without risking ambiguity, we avoid using the subperiod index $s$ or the time index $j$ or $t$, for example, a single value from the coarse time series could be denoted as $x^{(k)}$ instead of $x_s^{(k)}(j)$.

### 2.2. Disaggregation Kernels

Precise stochastic models, used as disaggregation kernels, can be constructed based on the premise that an arbitrary process $\{X(t)\}$ with any prescribed marginal distribution $F_X(x)$ having any valid (positive definite) linear ACS $\rho_X(\tau)$ can emerge by transforming a parent-Gaussian process $\{Z(t)\}$ having a standard Gaussian marginal $\Phi_Z(z)$ and an ACS $\rho_Z(\tau)$ that needs to be specified. In general, any nonlinear transformation $g(Z(t)) : R \rightarrow R$ applied to a Gaussian process modifies not only the marginal distribution but also the ACS $\rho_Z(\tau)$ by causing a decrease in its strength, which depends on the mathematical from of the transformation; that is, for an arbitrary bivariate normally distributed vector $(Z(t), Z(t-\tau))$ it is proven that $\mathrm{Cor}(g(Z(t)), g(Z(t-\tau))) \leq \mathrm{Cor}(Z(t), Z(t-\tau))$ (Kendall & Stuart, 1979, p. 600). It is well known that the marginal-back transformation $g(Z) \coloneqq Q_X(\Phi_Z(Z))$, where $Q_X$ is quantile function of $F_X(x)$, transforms the Gaussian r.v. $Z$ into the r.v. $X$. Thus, simulating the process $\{X(t)\}$ only requires the assessment of an autocorrelation transformation function $T$ such $\rho_Z(\tau) = \mathcal{T}(\rho_X(\tau))$; $\mathcal{T}$ takes as argument the target ACS and returns the inflated ACS of the Gaussian process.

For a unified account of this framework that enables fast and easy estimation of the parent-Gaussian process based on simple analytical correlation transformation functions and for applications in hydroclimatic processes see Papalexiou (2018) and references therein. However, to make this paper standalone, we provide a brief summary and an explanatory application of the procedure for fitting a stochastic model that generates time series with any marginal distribution (including mixed-type marginals to account for intermittency) and any valid (positive definite) linear correlation structure. Particularly:

(a) We assess the marginal distributions $F_{X_s}(x)$ and the ACSs $\rho_{X_s}(\tau)$ of each of the $N$ stationary target processes $\{X_s(t)\}$ at the time scale $k_0$. This can be done using observed data at the target fine scale $k_0$.

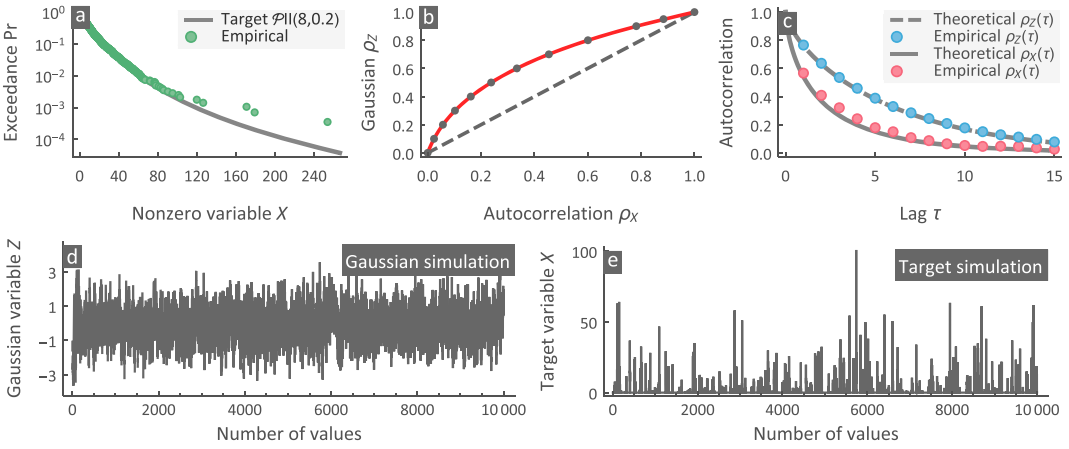


**Figure 1.** (a) The target marginal distribution $\mathcal{P}\text{II}(8, 0.2)$ for nonzero values compared with the empirical distribution of the target simulation, (b) the fitted autocorrelation transformation function, (c) the target ACS $\rho_X(\tau)$ and the inflated parent Gaussian $\rho_Z(\tau)$ compared with the corresponding empirical ones from the simulations, (d) simulation of Gaussian time series, and (e) simulation of the target variable.

If data are not available at the location of interest, the distribution and the ACS can be assessed based on regional information of near stations that show similar statistical behavior at the coarse time scale, or, by using scaling laws to infer the statistical properties of the process at the target scale $k_0$.

(b) For each target $\{X_s(t)\}$ process we estimate the autocorrelation transformation function

$$\rho_Z = \mathcal{T}_s(\rho_X; b, c) = \frac{(1 + b\rho_X)^{1-c} - 1}{(1 + b)^{1-c} - 1} \tag{5}$$

which creates a link between autocorrelation values of the target and the parent Gaussian process; for technical details on how this function is fitted see Papalexiou (2018).

(c) The ACS of the parent-Gaussian processes $\{Z_s(t)\}$ is now simply estimated by $\rho_{Z_s}(\tau) = \mathcal{T}_s(\rho_{X_s}(\tau); b, c)$, and the process is simulated using autoregressive models AR($p$) of sufficiently large order $p$ to reproduce the $\rho_{Z_s}(\tau)$.

(d) The generated Gaussian time series are transformed into the target time series by applying the corresponding marginal-back transformations, that is, $X_s = Q_{X_s}(\Phi_Z(Z))$, where $Q_{X_s}$ denote the quantile functions estimated from step (a).

We illustrate the previous steps with an example. Let us target to generate synthetic time series from an intermittent process (e.g., it could be precipitation) with probability zero $p_0 = 0.90$ and nonzero values following a Pareto II distribution $F_{\mathcal{P}\text{II}}(x) = 1 - (1 + \gamma\, x/\beta)^{-1/\gamma}$ with $(\beta, \gamma)$ = (8,0.2) (Figure 1a), and ACS described by the Weibull parametric form $\rho_X(\tau) = \rho_W(\tau) = \exp(-(\tau/b)^c)$ with $(b, c)$ = (5,0.7) (Figure 1c, solid grey line). Estimation of the autocorrelation transformation function (Figure 1b, red line) allows the assessment of the parent Gaussian ACS, that is, $\rho_Z(\tau) = \mathcal{T}(\rho_W(\tau); 23.3, 0.77)$ (Figure 1c, dashed grey line). Then, an AR(20) model is used to reproduce inadequately the $\rho_Z(\tau)$ (for $\tau > 20$ the $\rho_Z \approx 0$) and generate Gaussian time series (Figure 1d). Finally, the Gaussian time series are transformed to the target-variable times series (Figure 1e) by applying the marginal-back transformation using of course the mixed-type quantile in this case, that is, for $z \le z_{p_0} = Q_Z(p_0)$ ($Q_Z$ is the quantile function of the standard Gaussian variable) $x = 0$, while for $z > z_{p_0}$, $x = Q_{\mathcal{P}\text{II}}((\Phi_Z(z) - p_0)/(1 - p_0))$. For verification we show the empirical distribution of the synthetic time series (Figure 1a, green dots), as well as the empirical ACSs of the Gaussian (Figure 1c, blue dots) and synthetic time series (Figure 1c, red dots).

### 2.3. A Bernoulli-Trial Framework for Efficient Optimization

Previously, we described how to generate random sequences (time series) with any given linear ACS and marginal distribution. Now if we target to disaggregate a value $x^{(k)}$ (target value hereafter; subperiod and

time indicators $s$ and $j$ are omitted for notational simplicity) into a $k$-block $\boldsymbol{x} \coloneqq \{x(i)\}_{i=1}^{k}$ then by definition we desire $\sum_{i=1}^{k} x(i) = x^{(k)}$ for totals, or $1/k\sum_{i=1}^{k} x(i) = x^{(k)}$ for the average process. Clearly, a generated random $k$-block cannot sum (or average) exactly to the target value $x^{(k)}$ by chance. Particularly, let $\widehat{\boldsymbol{x}} \coloneqq \{\widehat{x}(i)\}_{i=1}^{k}$ denote a "candidate" random $k$-block with $\sum_{i=1}^{k} \widehat{x}(i) = \widehat{x}^{(k)}$ having a distance error from the target value $x^{(k)}$ equal to $\epsilon \coloneqq |x^{(k)} - \widehat{x}^{(k)}|$. Now we aim to find a $k$-block $\widehat{\boldsymbol{x}}$ with $\epsilon \le p_\epsilon \mid x^{(k)} \mid$, where $p_\epsilon$ is a small value (essentially $p_\epsilon$ is the relative error as $p_\epsilon \le |1 - \widehat{x}^{(k)}/x^{(k)}|$). Essentially, the optimization part aims to find a specific $k$-block, which has a small relative error, that is, sums close enough to the target value. Although an analytical solution does not exist to specify the $\widehat{\boldsymbol{x}}$ $k$-block, here, we show that within a Bernoulli-trial framework we can form a precise procedure that enables to find a $k$-block having any prescribed error $\epsilon$, that is, to sum (or average) as close as we wish to the target value. Here we use two common optimization methods:

Method 1: A sufficiently large number $v$ of random $k$-blocks is generated, and the one with the smallest $\epsilon$ is selected. Particularly, we generate $v$ random $k$-blocks, estimate their totals (or average values), calculate their error from the target value, and end up with a list of errors $\{\epsilon_1, \ldots, \epsilon_v\}$. The $k$-block corresponding to the smallest error among the $\{\epsilon_1, \ldots, \epsilon_v\}$ is selected.

Method 2: Iterate until the error goal is fulfilled by allowing a maximum number of $v$ iterations. Particularly, a first random $k$-block is generated and its error $\epsilon_1$ from the target value estimated. If the error goal is fulfilled, that is, $\epsilon_1 \le p_\epsilon \mid x^{(k)} \mid$, then this random $k$-block is selected; if not, a second $k$-block is generated and its error $\epsilon_2$ is compared with the error goal, and so on; that is, the procedure is repeated until a $k$-block is found to fulfill the error goal. To avoid infinite iterations, a "global" maximum number of iterations $v$ must be set. Thus, this procedure will create a list of errors $\{\epsilon_1, \ldots, \epsilon_i\}$ with $i \le v$ as the error goal is fulfilled in general before the maximum number of iterations is reached; however, if the maximum number of iterations is reached, then the $k$-block corresponding to the smallest error among the $\{\epsilon_1, \ldots, \epsilon_v\}$ is selected.

A major difference between these two approaches is that in Method 1 exactly $v$ $k$-blocks are generated and among them it is likely to observe more than one block fulfilling the error goal; in contrast, in Method 2 only one $k$-block (or zero if $v$ iterations are reached) fulfills the error goal (that is by the definition of the method). This results the selected $k$-block from Method 1 to have typically smaller error $\epsilon$ compared to the one from Method 2, as in the former case the best $k$-block is chosen (typically) among more than one block that fulfill the error goal, or else, in Method 1 the selected $k$-block is chosen from a larger pool of blocks than in Method 2, and this increases the chances to find one with even smaller error (this is further shown in section 2.4 and in Figures 3e and 3f). Note that a crucial aspect of the operational use of these methods is their implementation speed. The current technology of parallel processing or graphics processing unit programming assures that Method 1 can also be fast as it can be fully "parallelized," that is, in an $n$-core system the algorithm is $n$ times faster compared to a single-core system. Method 2 has a sequential structure (iterations until the error goal is achieved), and thus, it is not certain that it can be implemented exploiting fully the benefits of parallel computing.

Clearly, the goal in both methods is to specify the number $v$. If a target value $x^{(k)}$ is feasible to emerge by summing a random $k$-block, then the larger the number of generated blocks implies a larger probability to find a $k$-block with a smaller error $\epsilon$, that is, $\lim_{v \to \infty} \min\{\epsilon_1, \ldots, \epsilon_v\} = 0$, or else, the minimum error $\epsilon$ will converge to 0 (see Figure 2a). For operational use, however, it is impossible to generate an infinite number of random $k$-blocks (or for Method 2 we need to set a maximum number of iterations $v$ to avoid infinite or time-consuming loops), and thus, it is mandatory to assess the number of $k$-blocks or iterations needed to achieve the prescribed error with a given certainty. Clearly, a smaller $p_\epsilon$ demands (on average) a larger $v$, which however, is affected by the target value $x^{(k)}$ itself, for example, if $x^{(k)}$ belongs in an interval around the mode of the r.v. $X^{(k)}$ then the $\min\{\epsilon_1, \ldots, \epsilon_v\}$ converges faster to 0 as $v$ increases (Figure 2a, blue line), while if $x^{(k)}$ is an extreme value, then the convergence is much slower (Figure 2a, red line). Let as assume that $\widehat{x}^{(k)} \in A$ if $(1 - p_\epsilon)$ $x^{(k)} \le \widehat{x}^{(k)} \le (1 + p_\epsilon)x^{(k)}$, which implies that any value $\widehat{x}^{(k)} \in A$ has error $\epsilon = \left|x^{(k)} - \widehat{x}^{(k)}\right| \le p_\epsilon \, |x^{(k)}|$ fulfilling thus the error goal; now, given the distribution function of $X^{(k)}$ the probability to observe a value $\widehat{x}^{(k)} \in A$ is

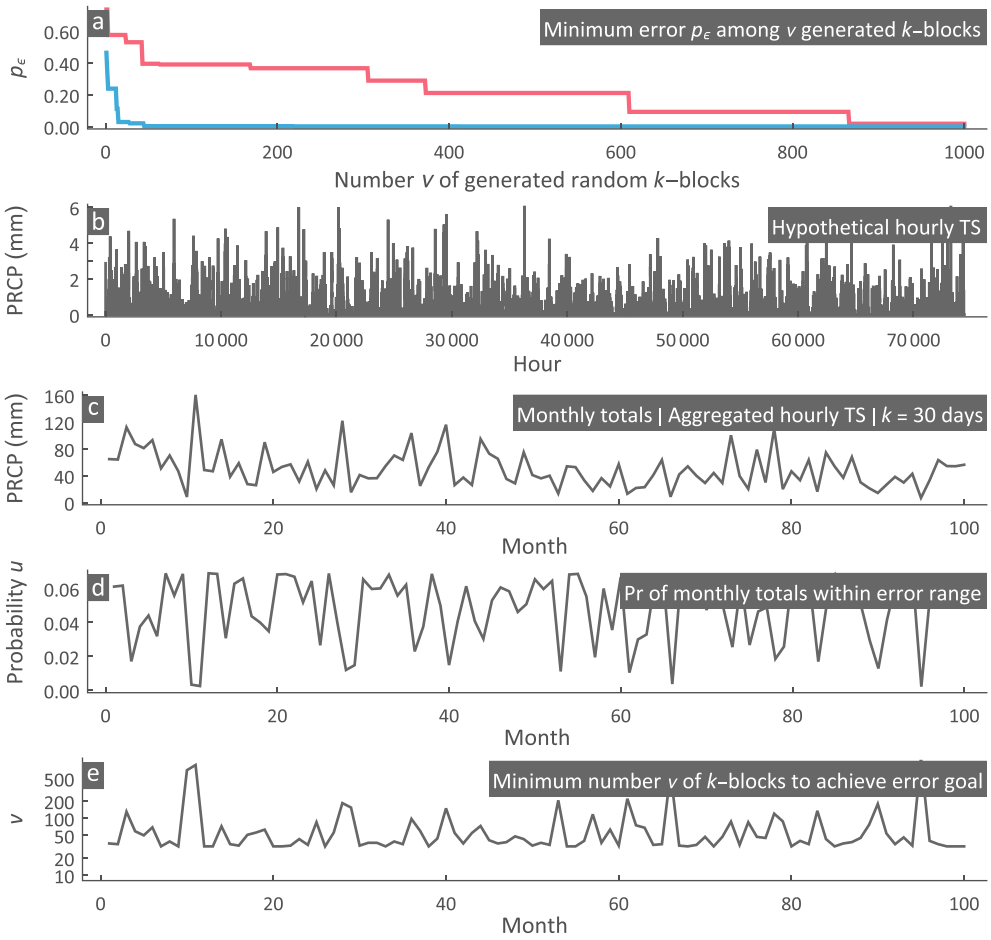


**Figure 2.** (a) The minimum relative error value $p_\epsilon$ estimated from sets of $v$ generated $k$-blocks showing its convergence to zero as $v$ increases; also, the $p_\epsilon$ converges faster to zero (blue line) for a target value with exceedance probably 0.5 (more probable) and much slower (red line) for one with 0.001 (extreme value); (b) a benchmark hypothetical hourly precipitation (PRCP) time series, and (c) the corresponding aggregated time series at the monthly time scale; (d) probabilities of the r.v. $X^{(k)}$ to belong in the interval $[(1-p_\epsilon)x^{(k)}, (1+p_\epsilon)x^{(k)}]$ with $p_\epsilon$ = 5% for the the monthly values $x^{(k)}$ shown in panel c, (e) minimum number $v$ of $k$-blocks or iterations needed to assure with probability 99% that $\epsilon \le p_\epsilon \cdot |x^{(k)}|$ for $p_\epsilon$ = 5%.

$$u = F_{X^{(k)}}\left((1+p_\epsilon)x^{(k)}\right) - F_{X^{(k)}}\left((1-p_\epsilon)x^{(k)}\right) \tag{6}$$

In terms of Bernoulli trials, we consider "success" $X^{(k)} \in A$ with probability $u$, and "failure" $X^{(k)} \notin A$ with probability $1-u$, and therefore, the probability to have at least one success in $v$ independent trials is $P = 1-(1-u)^v$. In the disaggregation scheme a candidate random $k$-block is generated, and then, summed (or averaged) to $\widehat{x}^{(k)}$ in order to be compared with the target value $x^{(k)}$. Thus, if we aim for an error $\epsilon \le p_\epsilon \mid x^{(k)}|$ with 100$P$% confidence (certainty), we have to generate at least a number of $k$-blocks equal to

$$v = \frac{\ln(1-P)}{\ln(1-u)} \tag{7}$$

with $u$ given from equation (6).

Accurate estimation of $u$ needs the distribution function of the r.v. $X^{(k)} = \sum_{i=1}^{k} X(i)$. We can simply estimate $F_{X^{(k)}}(x)$ by sampling a large number of $k$-blocks from the disaggregation kernel and by summing (or averaging) them to obtain $\widehat{x}^{(k)}$ values; then it is straightforward to fit an appropriate parametric distribution to the sample of $\widehat{x}^{(k)}$ values. For example, assuming a hypothetical hourly precipitation time series (Figure 2b) and its monthly ($k$ = 30 · 24 hr) aggregated counterpart (Figure 2c), we fit the $F_{X^{(k)}}(x)$ with the

aforementioned method and we estimate the corresponding probabilities $u$ for each monthly value and for $p_\epsilon = 5\%$ (Figure 2d); finally, we estimate the minimum number of $v$ blocks or iterations needed to achieve the error goal with 99% confidence (Figure 2e). Of course, an extremely large $v$ would cause a significant delay; thus, a global maximum $v_{max}$ should always be set; for example, using the estimated $v$ values we can a set a global maximum so 99% of $v$ values are less than it (in this example $v_{max} = 361$).

### 2.4. Effects of the Correction Factor

Previously, we showed that if we target to disaggregate a value $x^{(k)}$ into a $k$-block, we can find a candidate $k$-block $\widehat{\boldsymbol{x}}$ (emerging from a process with desired ACS and marginal distribution), which sums to a value close to $x^{(k)}$, that is, $\sum_{i=1}^{k}\widehat{x}(i) = \widehat{x}^{(k)} \approx x^{(k)}$. The Bernoulli framework we introduced enables to calculate the number $v$ of $k$-blocks we need to generate (or the number of iterations) in order to find one (with given confidence) that has any prescribed error $\epsilon := \left|x^{(k)} - \widehat{x}^{(k)}\right| \le p_\epsilon \,|\, x^{(k)} \,|$. Clearly, it is not optimal to generate an extremely large number of $k$-blocks in order to find the one that sums extremely close to $x^{(k)}$, yet we can find one with an acceptable error, and if we wish, we can eliminate this error $\epsilon$ simply by multiplying the values of the selected $k$-block $\widehat{\boldsymbol{x}}$ by the correction factor $c_\epsilon := |\, x^{(k)}/\widehat{x}^{(k)} \,|$. Now an important question is if this correction is meaningful; we deem that essentially it is not if the prescribed error is small. For example, disaggregating with a small relative error $p_\epsilon = 5\%$, it is hard to argue on what practical difference it makes, for example, if a generated hourly precipitation block, aiming to disaggregate a monthly value of 10 mm, totals somewhere in the range $10 \pm 0.5$ mm (measurement errors could be even larger than this). However, since it has been a common practice to correct the disaggregated values to match exactly the target value, probably because the computing power in the past did not allow to find blocks with small error, we provide here a framework to assess the effects of this correction in the distributional properties of the disaggregated time series.

Particularly, rescaling an r.v. $X$ by multiplying it by the numerical value $c_\epsilon$ affects its properties, for example, the r.v. $c_\epsilon X$ has mean and standard deviation $c_\epsilon \mu_X$ and $c_\epsilon \sigma_X$, respectively (where $\mu_X$ and $\sigma_X$ denote the mean and standard deviation of the r.v. $X$). In Figures 3a and 3b we show time series generated by disaggregating the monthly totals in Figure 2c using the two optimization methods, while Figures 3c and 3d shows the correction factors for each $k$-block disaggregating the monthly values. The resulting $c_\epsilon$ factors exhibit bell-shaped and uniform distributions for Methods 1 and 2, respectively, which also verifies (as aforementioned in the previous section) that the error from method 1 is typically smaller than that of Method 2 (see histograms of Figures 3e and 3f). This is expected as in Method 2 the first $k$-block with error $\epsilon \le p_\epsilon \,|\, x^{(k)} \,|$ ends the optimization while in Method 1 typically more than one $k$-block fulfills the error goal and the best of them is selected. Now given that each $k$-block is rescaled with a different $c_\epsilon$ we can investigate the effects of this correction by assuming that $c_\epsilon$ is an r.v. itself; thus, the r.v. describing the final disaggregated time series could be expressed by the r.v. $W = C_\epsilon X$. We can show that the error correction factor $c_\epsilon$, given that $\epsilon \le p_\epsilon \cdot |\, x^{(k)} \,|$, is confined in $[(1 + p_\epsilon)^{-1}, (1 - p_\epsilon)^{-1}]$, while to ease the mathematical analysis we investigate the second case (Method 2) where we can assume that $C_\epsilon$ is distributed uniformly within this range (see Figure 3f), that is, $C_\epsilon \sim \mathcal{U}\left((1 + p_\epsilon)^{-1}, (1 - p_\epsilon)^{-1}\right)$. Now if $f_X(x)$ and $f_{C_\epsilon}(c_\epsilon)$ are the pdf's of $X$ and $C_\epsilon$, respectively, and $X$ and $C_\epsilon$ are assumed to be independent, then the pdf of $W$ is given by

$$f_W(w) = \int_{-\infty}^{\infty} f_X(x) f_{C_\epsilon}(w/x)\, |x|^{-1}\, \mathrm{d}x \tag{8}$$

This enables us to compare the r.v.'s $X$ and $W$, quantify the effect of this correction, and finally assess the relative error $p_\epsilon$ value that does not modify the properties of $X$.

In order to demonstrate this framework, we use a versatile three-parameter distribution (any other distribution can be used), which we apply in all case studies, that is, the generalized gamma ($\mathcal{GG}$) distribution (Papalexiou & Koutsoyiannis, 2012, 2016; Stacy, 1962) with pdf

$$f_{\mathcal{GG}}(x;\beta,\gamma_1,\gamma_2) = \frac{\gamma_2}{\beta\,\Gamma(\gamma_1/\gamma_2)} \left(\frac{x}{\beta}\right)^{\gamma_1 - 1} \exp\left(-\left(\frac{x}{\beta}\right)^{\gamma_2}\right) \tag{9}$$

where $\beta > 0$ is a scale parameter, $\gamma_1 > 0$ and $\gamma_2 > 0$ are shape parameters, and $\Gamma(\cdot)$ is the gamma function. For $\gamma_1 < 1$ and $\gamma_1 > 1$ the pdf is J- and bell-shaped, respectively, while the parameter $\gamma_2$ adjusts mainly the

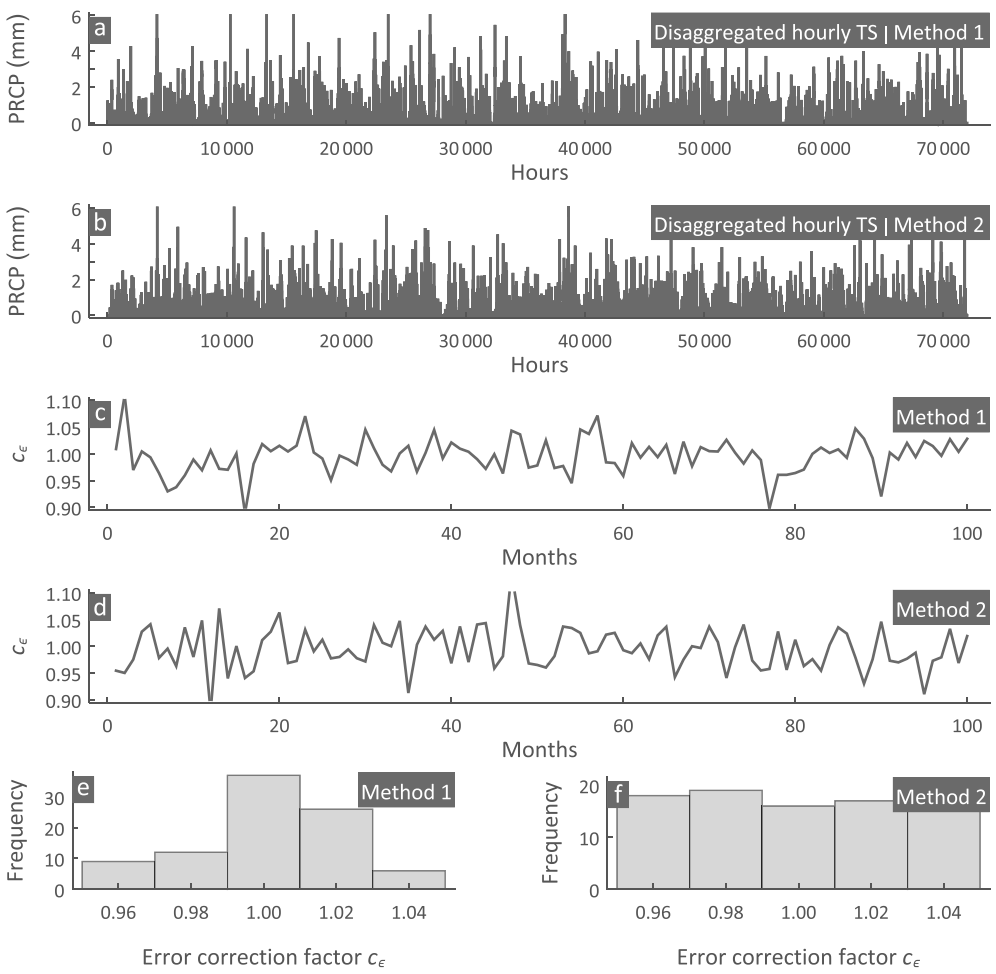


**Figure 3.** (a and b) Hourly time series generated by disaggregating the monthly totals shown in Figure 2c; (c and d) error correction factors $c_\epsilon$ for each hourly block disaggregating the corresponding monthly values; (e and f) corresponding histograms of the $c_\epsilon$ values shown in panels c and d. Method 1 disaggregates a target value by generating $\nu$ $k$-blocks and choosing the one with the smaller error, while Method 2 is a trial-and-error iteration framework seeking the first block to fulfill the error goal and allowing a maximum of $\nu$ iterations.

"heaviness" of the right tail, and thus, the behavior of extreme events. Applying equation (9) for $X \sim \mathcal{GG}(\beta, \gamma_1, \gamma_2)$ and $C_\epsilon \sim \mathcal{U}\left((1+p_\epsilon)^{-1}, (1-p_\epsilon)^{-1}\right)$ we get

$$f_W(w) = \left(1-p_\epsilon^2\right) \frac{\Gamma\left(\frac{\gamma_1-1}{\gamma_2}, \left((1-p_\epsilon)\frac{w}{\beta}\right)^{\gamma_2}\right) - \Gamma\left(\frac{\gamma_1-1}{\gamma_2}, \left((1+p_\epsilon)\frac{w}{\beta}\right)^{\gamma_2}\right)}{2p_\epsilon \beta \Gamma(\gamma_1/\gamma_2)} \tag{10}$$

with $\lim_{p_\epsilon \to 0} f_W(w) = f_X(x)$. For example, for $X \sim \mathcal{GG}(0.5, 1, 0.6)$ using equation (10) we can plot and compare the pdf's for various values of $p_\epsilon$, that is, $p_\epsilon = \{5,\ 10,\ 20,\ \text{and } 30\%\}$. We see (Figure 4a) that the pdf's $f_W(w)$ are almost identical with $f_X(x)$ and the difference is only revealed if we plot the distribution function difference $\Delta F := F_X(x) - F_W(w)$ (Figure 4b), which clearly indicates very small deviations even for $p_\epsilon$ = 10%; for $p_\epsilon$ = 5%, the difference is essentially zero. Of course, different distributions may show larger deviation for the same $p_\epsilon$ values; for example, selecting a bell-shaped $\mathcal{GG}(0.5, 3, 0.6)$ we observe (Figure 4c) more apparent differences in the pdf's, yet $\Delta F$ is still very small for $p_\epsilon$ = 10% and essentially zero for $p_\epsilon$ = 5% (Figure 4d). Also, note that $\Delta F$ is not constant in the whole r.v. range but peaks at some value close to the mean of $X$ and vanishes for large values. As already mentioned, the choice of the pdf $f_X(x)$, as well as the values of its parameters, can affect the difference $\Delta F$, yet it is rational to expect that an a priori selected small $p_\epsilon$ like 5% is a safe choice. Of course, what is considered a safe choice is subjective as it also depends on the $\Delta F$ we are willing to accept.

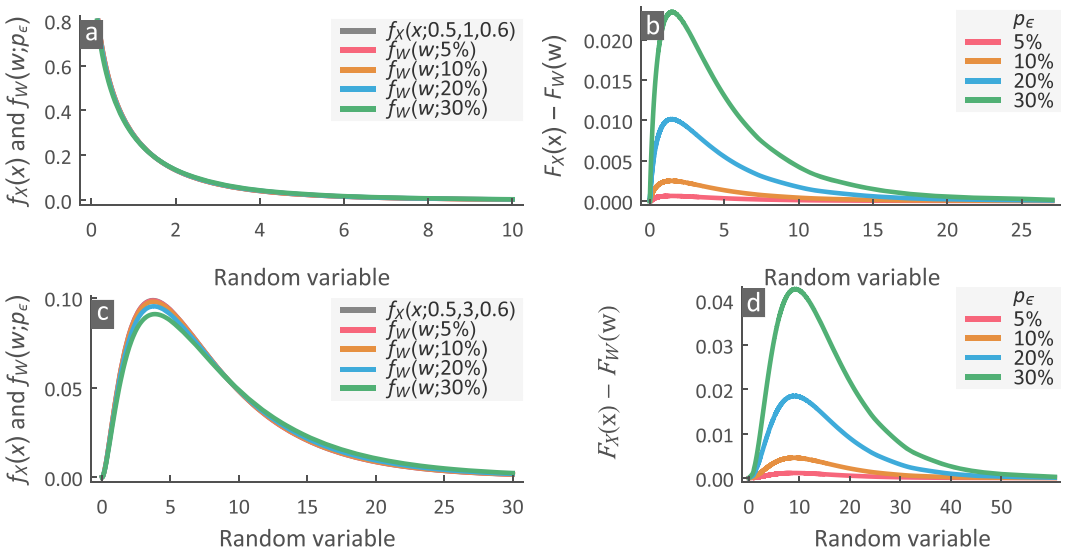


**Figure 4.** Comparison of the r.v.'s $X$ and $W = C_\epsilon \cdot X$ for various relative error values $p_\epsilon$ in terms of pdf's and cdf differences for: (a and b) a J-shaped generalized gamma and (c and d) a bell-shaped generalized gamma.

Finally, we note that the previous analysis cannot be easily performed assuming a normal distribution for $c_\epsilon$ (Method 1), as the corresponding product r.v. $W = C_\epsilon X$ does not have an analytical form. Yet it should be clear that $\Delta F$ is expected to be even smaller in this case, as there are more values close to 1 (which implies less disturbance; Figure 3e) and less values in the edges of the $[(1 + p_\epsilon)^{-1}, (1 - p_\epsilon)^{-1}]$ range.

### 2.5. Blueprint for Stationary and Nonstationary Disaggregation

Summarizing and linking the methods described in the previous sections, we provide here a complete operational scheme, in order to disaggregate a given coarse-scale time series $\{x_s^{(k)}(j)\}$ into a fine-scale time series $\{x_s(t)\}$ generated from a cyclostationary process $\{X_s(t)\}$ with prescribed stochastic characteristics. Particularly:

1. Define (assess) the marginal distributions $F_{Xs}(x)$ and the ACSs $\rho_{Xs}(\tau)$ at the target fine time scale, and the corresponding parent-Gaussian ACSs $\rho_{Zs}(\tau)$. Then fit $AR_s(p)$ models of sufficiently large order $p$ that reproduce the $\rho_{Zs}(\tau)$ ACSs (see section 2.2).
2. Choose a desired relative error $p_\epsilon$ (e.g., 5%) and estimate for each target value $x_s^{(k)}(j)$ the number $v$ of random $k$-blocks (or iterations) that have to be generated in order to find at least one fulfilling the prescribed $p_\epsilon$ with given confidence $P$, for example, $P$ = 99% (section 2.3).
3. For a target value $x_s^{(k)}(j)$ generate $v$ random Gaussian blocks $\widehat{\boldsymbol{z}}_s(j) \coloneqq \{\widehat{z}_s(t)\}_{t=(j-1)k+1}^{jk}$ using the fitted $AR_s(p)$ model.
4. The $v$ generated $\widehat{\boldsymbol{z}}_s(j)$ blocks are transformed into $\widehat{\boldsymbol{x}}_s(j) \coloneqq \{\widehat{x}_s(t)\}_{t=(j-1)k+1}^{jk}$ blocks by using the transformation $\widehat{x}_s(t) = Q_{X_s}(\Phi_Z(\widehat{z}(t)))$.
5. The sum (or average) of each $\widehat{\boldsymbol{x}}_s(j)$ block is estimated, that is, $\Sigma_{t=(j-1)k+1}^{jk} \widehat{x}_s(t) = \widehat{x}_s^{(k)}(j)$, in order to calculate a list of $v$ errors $\epsilon = |x_s^{(k)}(j) - \widehat{x}_s^{(k)}(j)|$ from the target value.
6. The $\widehat{\boldsymbol{x}}_s(j)$ block corresponding to the smallest error $\epsilon$ is selected.
7. The values of the selected $\widehat{\boldsymbol{x}}_s(j)$ block are multiplied by the error correction factor $c_\epsilon \coloneqq |x_s^{(k)}(j)/\widehat{x}_s^{(k)}(j)|$ so that $\Sigma_{i=1}^{k} \widehat{x}_s(i) = x_s^{(k)}(j)$.
8. The next target value $x_s^{(k)}(j+1)$ is disaggregated by repeating steps (3–7).

To provide some remarks for the application of the scheme, we note that first, if Method 2 is selected to disaggregate a target value $x_s^{(k)}(j)$, then steps (3–5) are modified accordingly; that is, a single $\widehat{\boldsymbol{z}}_s(j)$ is generated and transformed into $\widehat{\boldsymbol{x}}(j)$; then the $\epsilon = |x_s^{(k)}(j) - \widehat{x}_s^{(k)}(j)|$ is estimated, and if $\epsilon \leq p_\epsilon |x_s^{(k)}(j)|$, the process ends, otherwise is repeated for a maximum of $v$ iterations. In the case of reaching the maximum number of iterations $v$ and the error goal has not been achieved, then the block with the smallest error among the $v$ generated blocks is selected. Second, as the algorithm sequentially disaggregates the coarse scale values, it builds

up in parallel two time series, that is, the disaggregated one $\{x_s(t)\}$, but also the $\{z(t)\}$ comprising the corresponding Gaussian variable values, that is, those that were transformed to the final disaggregated values. This is necessary as the $AR_s(p)$ model uses always as starting values previous values of the $\{z(t)\}$ time series in order to preserve the correlation structure. Third, in the case of mixed-type r.v.'s like precipitation it is obvious that a zero precipitation value at the time scale $k$ is always disaggregated into a $k$-block of zero values, then obviously step (7) is omitted as $\widehat{x}_s^{(k)}(j) = 0$, and thus, the correction factor cannot be defined. Also, as previously noted, the use of the correction factor (step 7) is not strictly required and can be omitted if the prescribed error is negligible for all practical purposes.

Now the previously described scheme was based on the assumption that the disaggregation kernels are cyclostationary; that is, the stochastic process $\{X_s(t)\}$ is the same as the $\{X_s(t + n_p)\}$ process, where $n_p$ denotes the period. However, it is straightforward to modify this assumption and form a fully nonstationary framework. Particularly, we can assume (or define) that any of the stationary processes at the target time scale are nonstationary; that is, their stochastic characteristics change in a predefined way, and thus, are functions of time; in this case $\{X_s(t)\} \neq \{X_s(t + n_p)\}$. For example, we can define that statistical characteristics such as the mean, standard deviation, or shape measures change over time in a prescribed way, which in turn, allows the estimation of the marginal distributions $F_{Xs}(x)$ at any $t$ and consequently of the disaggregation kernels. We demonstrate the generality and the flexibility of this nonstationary framework is section 4.3.

As a general comment, we stress that this scheme is essentially parsimonious as the only true parameters we need to estimate are those that describe the process at the target fine scale, and that is, the parameters of the marginal distribution and of the ACS. For example, if one wishes to disaggregate monthly precipitation into hourly, assuming that in a given month the nonzero rainfall follows a Pareto II distribution (two parameters) and the ACS is described by a Weibull parametric form (two parameters), then the total number of parameters is four, plus one related to the estimation of probability dry. All the rest of the parameters used, for example, in the large order AR models, or in the Bernoulli framework, are not essentially parameters as they are deterministically defined (or entail) by the selection of the marginal and of the ACS. Clearly, these parameters should be estimated for any stationary period (e.g., month), and of course, additional parameters are needed when nonstationarity is assumed.

## 3. Stationary Disaggregation

### 3.1. Proof-of-Concept: Disaggregating Monthly Precipitation Into Hourly

As a proof-of-concept for illustrating the proposed method, we disaggregate monthly precipitation values into hourly. We use a randomly selected station (code: 3240_154202) from the hourly precipitation data set of National Climatic Data Center of the USA (see Hammer & Steurer, 1997) covering the period 1 February 1981 to 30 November 2011. As anticipated, the hourly precipitation time series and the corresponding monthly values exhibit different statistical properties (Figures 5a and 5b). The former is the result of an intermittent process with hourly probability dry ranging from 88 to 96% (depending on the month) and high positive skewness, while the latter can be characterized as continuous (all monthly values were found nonzero) with values tending towards normality due to the central limit theorem.

Following the steps described in section 2.5 we first assume hourly precipitation corresponding to each month as a stationary intermittent process; thus, for every month we estimate the probability dry $p_0$ and we fit the $\mathcal{GG}$ distribution (equation (9)) to describe the nonzero values. Its mean $\mu_{\mathcal{GG}}$, standard deviation $\sigma_{\mathcal{GG}}$, and coefficient of skewness $CS_{\mathcal{GG}}$ are given, respectively, by

$$\mu_{\mathcal{GG}} = \frac{\beta\Gamma\left(\frac{\gamma_1+1}{\gamma_2}\right)}{\Gamma\left(\frac{\gamma_1}{\gamma_2}\right)} \tag{11}$$

$$\sigma_{\mathcal{GG}} = \frac{\beta\left(\Gamma\left(\frac{\gamma_1+2}{\gamma_2}\right)\Gamma\left(\frac{\gamma_1}{\gamma_2}\right) - \Gamma\left(\frac{\gamma_1+1}{\gamma_2}\right)^2\right)^{1/2}}{\Gamma\left(\frac{\gamma_1}{\gamma_2}\right)} \tag{12}$$

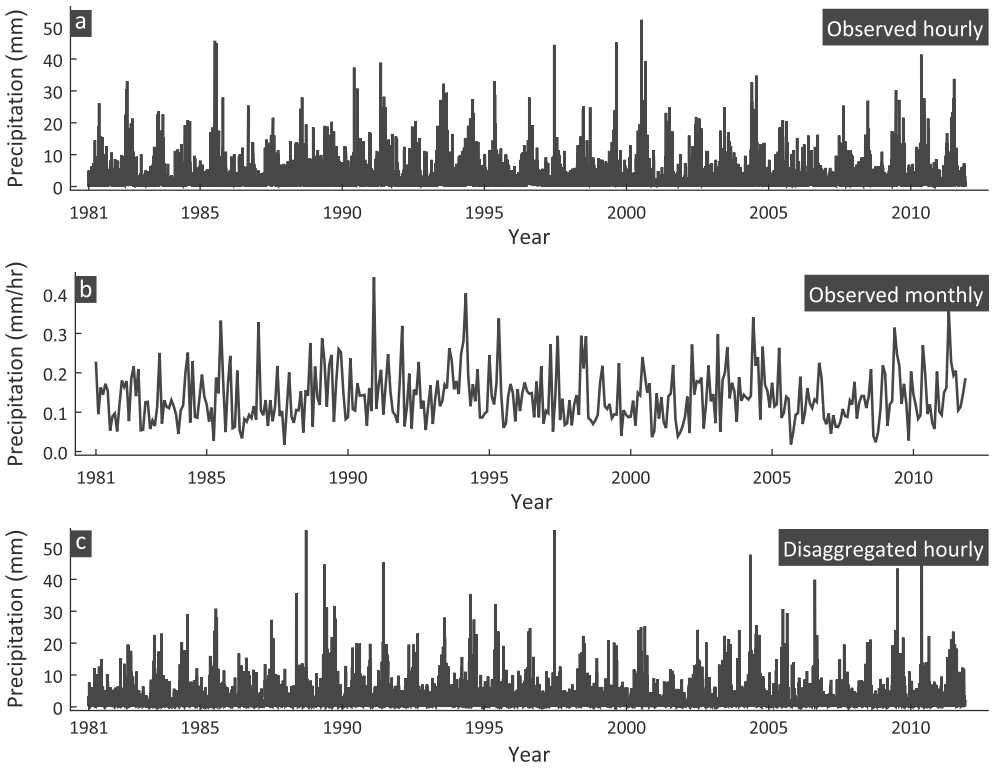


**Figure 5.** (a) Observed hourly precipitation, (b) the corresponding observed monthly (aggregated) time series, and (c) hourly precipitation time series created by disaggregating the monthly time series of panel b.

$$\mathrm{CS}_{\mathcal{GG}} = \frac{2\Gamma\left(\frac{\gamma_1+1}{\gamma_2}\right)^3 - 3\Gamma\left(\frac{\gamma_1+2}{\gamma_2}\right)\Gamma\left(\frac{\gamma_1}{\gamma_2}\right)\Gamma\left(\frac{\gamma_1+1}{\gamma_2}\right) + \Gamma\left(\frac{\gamma_1+3}{\gamma_2}\right)\Gamma\left(\frac{\gamma_1}{\gamma_2}\right)^2}{\left(\Gamma\left(\frac{\gamma_1+2}{\gamma_2}\right)\Gamma\left(\frac{\gamma_1}{\gamma_2}\right) - \Gamma\left(\frac{\gamma_1+1}{\gamma_2}\right)^2\right)^{3/2}} \tag{13}$$

Note that maximum likelihood led to parameter estimates indicating unrealistically heavy tails and theoretical $\mu_{\mathcal{GG}}$ and $\sigma_{\mathcal{GG}}$ values deviating significantly from the observed ones (that is probably due to the discretization errors of the hourly data especially for small values, i.e., the presence of the so-called statistical ties). For this reason, we fitted the $\mathcal{GG}$ using the method of moments (equations (11)–(13)), and thus, the emerging distributions preserve exactly these characteristics. Comparison of the empirical distributions with the fitted ones indicates an excellent agreement (see Figures 6a and 6b for a summer and winter month and Figure S1 for all months). Recalling that the parameter $\gamma_2$ controls the tail behavior, its range (0.41–0.92) indicates subexponential tails, and it is in agreement with an extensive analysis on hourly extremes based on more than 4,000 hourly precipitation records across the United States (Papalexiou et al., 2018).

Next we calculate the empirical autocorrelation values up to lag 15, as autocorrelation is essentially 0 for higher lags and for all months. Then, we fit a parametric power-type ACS (see Papalexiou, 2018, for details on parametric ACSs), that is, the Pareto II, given by

$$\rho_{\mathrm{PII}}(\tau; b, c) = \left(1 + c\frac{\tau}{b}\right)^{-1/c} \tag{14}$$

where $b > 0$ and $c > 0$. This parametric ACS interpolates the empirical values almost perfectly in all months (see Figures 6c and 6d and S2 for all months). For demonstration, we depict also the parent-Gaussian ACS (dashed line in Figures 6c and 6d and S2), which is highly inflated as expected.

Finally, we reproduce the parent-Gaussian ACSs of each month by using an AR($p$) model of order $p = 72$ (i.e., taking into account the previous 72 hr of precipitation) as the parent-Gaussian ACSs of some months show

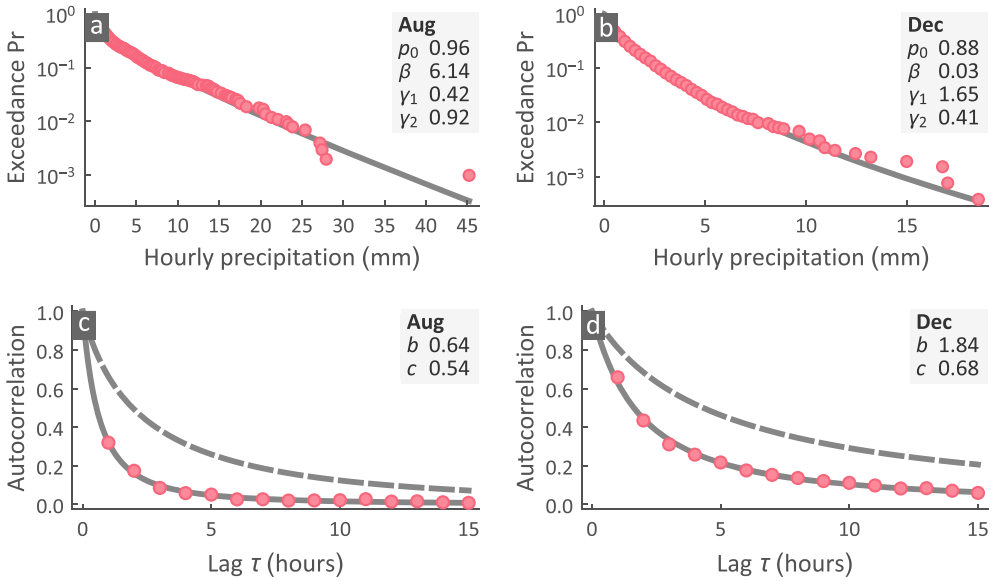


**Figure 6.** (a and b) Empirical distributions (red dots) of observed nonzero hourly precipitation (Figure 5a) and the fitted generalized gamma ($\mathcal{GG}$) distributions (solid line) for a summer and a winter month; the legend shows the probability dry $p_0$ and the estimated $\mathcal{GG}$ parameters. (c and d) Empirical autocorrelation structure (ACS) (red dots) of the observed hourly precipitation (Figure 5a), the fitted parametric Pareto II (PII) ACS (solid line), and the ACS of the parent-Gaussian process (dashed line); the legend shows the estimated parameters of the fitted PII ACS.

positive correlations up to this lag. We stress again the parsimonious character of this model, as the $p$ coefficients of the AR($p$) model are analytically determined by the parent-Gaussian ACS, which in turn emerges by the fitted two-parameter PII ACS in this case; thus, the Gaussian process model is essentially a two-parameter model. Subsequently, we disaggregate the monthly time series (Figure 5b) according to the steps in section 2.5 and we obtain the disaggregated time series (Figure 5c).

A first inspection of the observed (Figure 5a) and the disaggregated time series (Figure 5c) shows a remarkable similarity. Yet we assess in detail the statistical quality of the disaggregated time series by comparing the empirical distribution and the ACS of the synthetic time series with those of the target (observed) series. Referring to Figures 7a and 7b for two characteristic months and Figure S3 for all months, the empirical distributions (blue dots) of the disaggregated data match very well the target distributions (solid lines) that were fitted using the observed data. Of course, minor deviations on the tails are expected due to random variations and are not the result of a systematic error. Comparing the empirical ACSs (blue dots) with the target ACSs (solid line, Figures 7c and 7d and S4) also reveals an outstanding match with small deviation emerging by sampling fluctuations.

Finally, Figure 8 shows a side-by-side comparison of summary statistics between the observed and the aggregated time series for all months. Particularly, the probability dry, the mean, and the standard deviation are almost indistinguishable, while small deviations in skewness are due to sampling fluctuations. In fact, it is well known that sample estimates of skewness are not robust for samples drawn from highly skewed and subexponential distributions and in general should be avoided and alternatives like L-moments (Hosking, 1990; Lombardo et al., 2014; Papalexiou & Koutsoyiannis, 2016; Peel et al., 2001) should be preferred.

## 4. Treating Nonstationarity

By definition a stationary process has statistical properties that remain time invariant. In contrast, nonstationarity implies changes in the marginal distribution attributes such as the mean value, scale (standard deviation), and shape characteristics (e.g., heavier tails), and in the joint distributional properties often expressed by the ACS. This time-varying complexity creates difficulties in identifying the proper nonstationary model based on the limited information from the observed time series (see, e.g., Lins & Cohn, 2011; Serinaldi et al., 2018). Yet by necessity, nonstationary approaches (see, e.g., Cheng & AghaKouchak, 2014; Cheng

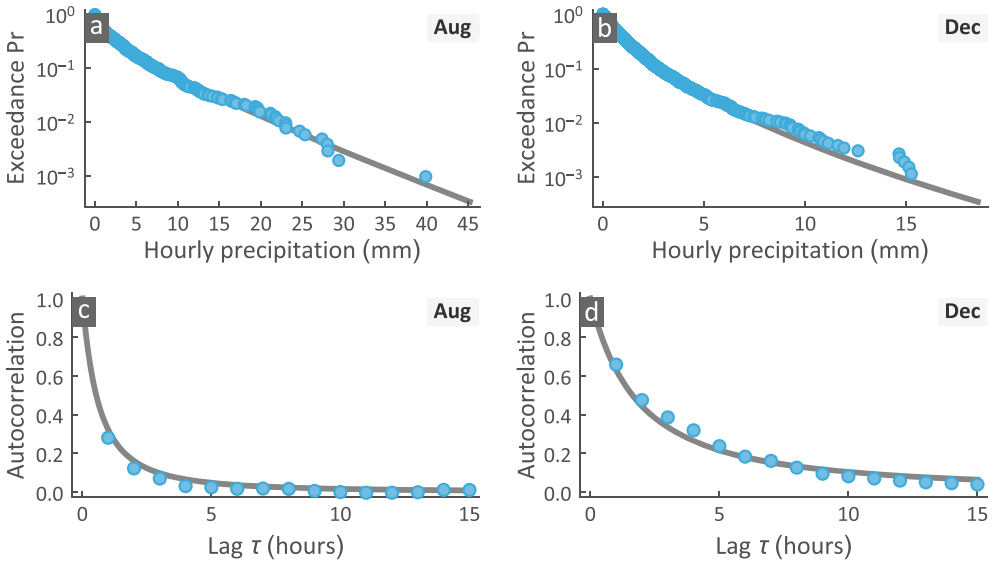


**Figure 7.** Verification of the statistical properties of the disaggregated hourly time series shown in Figure 5c. (a and b) Empirical distributions (blue dots) of disaggregated nonzero hourly precipitation in comparison with the target distribution (solid line) assessed from observed data (Figure 6a,b). (c and d) Empirical autocorrelation structure (ACS) of disaggregated hourly precipitation (blue dots) in comparison with the target ACS assessed from observed data (Figure 6c,d).

et al., 2014; Obeysekera & Salas, 2016; Ragno et al., 2018; Read & Vogel, 2016) often grounded on a priori assumptions about the specific attributes exhibiting a trend (e.g., trend in the mean) and the form of the trend (e.g., a linear trend). Developing nonparametric or adaptive methodologies for nonstationary modeling remains a challenge, but it is outside the scope of the present paper.

### 4.1. Crash Test: Adaptation of Stationary Kernels to Non-stationarity

In the previous section, we showed that the disaggregation scheme developed here can generate fine-scale time series consistent with a priori known marginal distribution and ACS. Yet an important question is how this scheme adapts under nonstationary conditions, and particularly, when nonstationarity is assumed for the process at the coarse scale, which also implies nonstationarity for the target (fine) scale. The purpose of this crash test is to investigate the disaggregation of a nonstationary process at the coarse (monthly) scale but using stationary kernels which will generate time series at the finer (daily) scale while preserving the

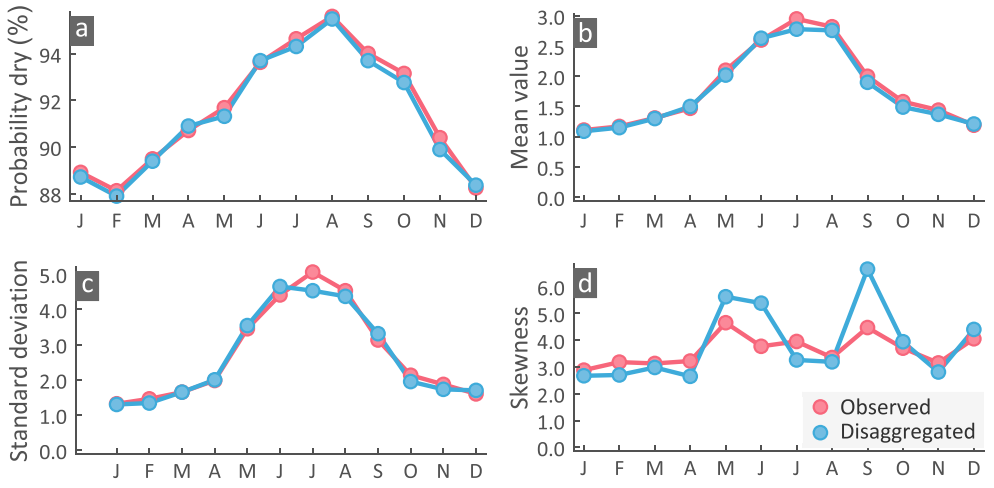


**Figure 8.** Observed hourly time series (Figure 5a) versus disaggregated (Figure 5c). Monthly comparison of (a) probability dry, (b) mean value, (c) standard deviation, and (d) skewness.

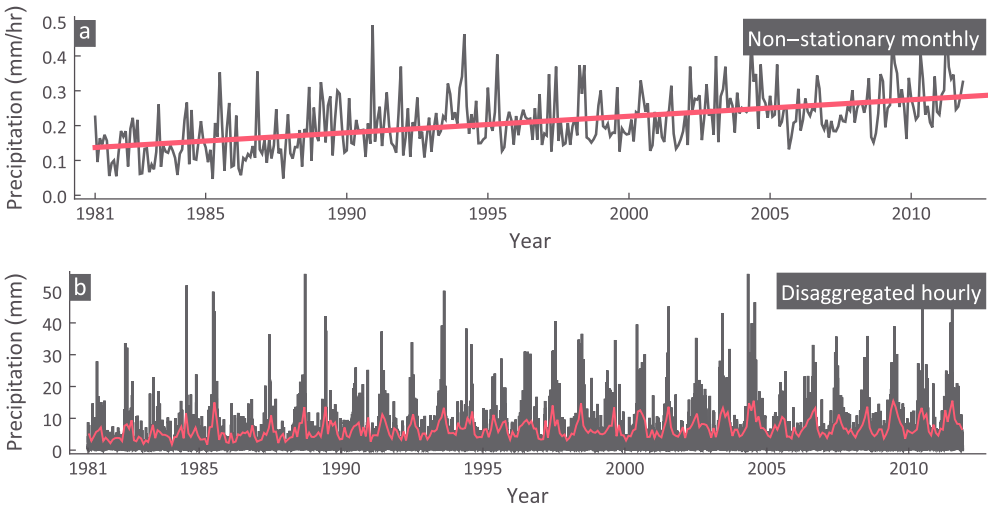


**Figure 9.** (a) A modified monthly time series exhibiting a trend (red line); (b) hourly precipitation time series created by disaggregating the monthly time series in panel (a) and the mean value of the largest 2% of hourly values (red line).

coarse-scale totals. This approach could be of practical interest when potential nonstationarity is observed at the coarse scale, yet the exact form of nonstationarity at the fine-scale cannot be robustly assessed, for example, due to insufficient information or lack of theoretical justification. Here we explore the most common case of nonstationarity consisting of a linear trend. Particularly, we assume that the monthly precipitation (Figure 5b) changes at a rate of 0.00039 mm/hr per month, that is, doubling its mean in 30 years (see Figure 9a). We disaggregate the trending time series by using the stationary disaggregation kernels described in section 3.1, that is, estimated from the observed hourly precipitation (Figure 5a).

The hourly disaggregated time series (Figure 9b) show the same pattern as the observed ones (Figure 5a). Still, a careful inspection shows an "intensifying" behavior over time, which is more apparent by depicting, for example, the monthly mean value of the largest 2% of hourly values (Figure 9b, red line). The estimated change, based on the fitted trend to the disaggregated values, is the same as in the monthly time series, that is, 0.14 mm/hr over a 30-year period.

A more detailed comparison shows (a) a decrease in probability dry (Figure 10a), especially for nonsummer months, (b) an increase in the mean of nonzero precipitation (Figure 10b) especially in summer, (c) standard

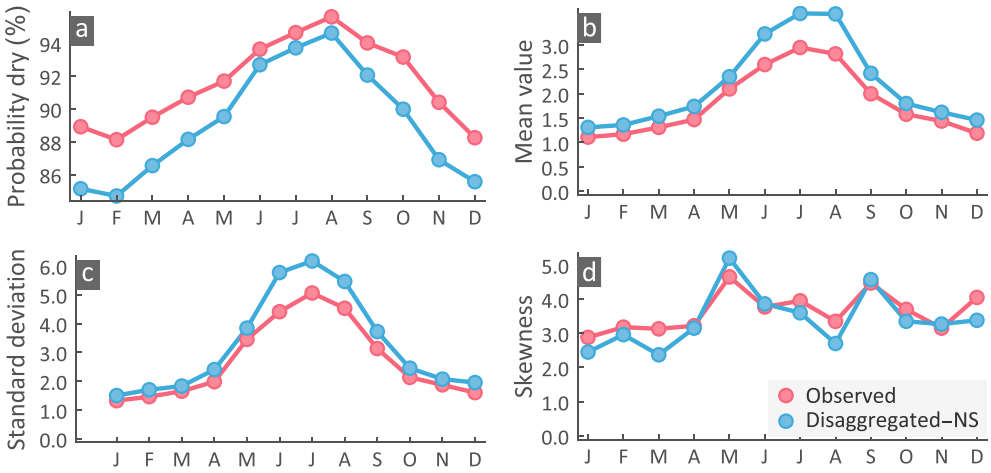


**Figure 10.** Observed hourly time series (Figure 5a) versus disaggregated (Figure 9b) from the modified monthly time series (Figure 9a). Comparison of (a) probability dry, (b) mean value, (c) standard deviation, and (d) skewness. Note that statistics shown for the nonstationary case express an average state.

deviation increases (Figure 10c) mainly in summer, and (d) no change in shape (Figure 10d) as quantified by the skewness coefficient, implying that more extreme values result by location and scale changes. Of course, the statistics shown in Figure 10 for the nonstationary case express an average stage as in reality these statistics should be time varying. This adaptation to nonstationarity is rational and anticipated, because feeding systematically larger monthly values in the disaggregation algorithm forces the selected random block to have either more wet days, or, larger values, or, both, in order to fulfill the constraint and add up to the monthly values. Clearly, since there is no reason for the procedure to choose one of these two options, we observe changes in both. The reason we observe a different "adaptation" over the summer months relates probably to the disaggregation kernels used; that is, the target stochastic processes for the summer months have the less intense ACS (see Figure S2) and this implies less variability in terms of probability dry, which in turn forces the process to choose blocks with larger nonzero values.

This crash test shows that although the disaggregation kernels are stationary, the optimization process creates a nonstationary process at the fine scale in order to respect the coarse-scale nonstationarities. Of course, this approach does not provide full control on the statistical properties that become nonstationary at the fine scale. For example, in this crash test we observed changes mainly in probability dry and the mean, yet we may wish to generate time series from a process where the shape characteristics also change; for the latter case the scheme using nonstationary kernels should be chosen. Finally, we stress that when we use stationary kernels, their properties (assessed e.g., from a past stationary period) should be generally nonvalid in the nonstationary projection period as changes in the coarse scale should be reflected also in the fine scale. The resulting nonstationarity in some statistical properties is a "by-product" due to the forcing constraints of the nonstationary coarse process. According to this argument, there is not a theoretical justification for the use of a kernel assessed by the historical marginals and ACS apart from the fact that it offers a rational starting point and probably a more robust option than "speculating" the future properties of a kernel without sufficient information. Clearly, any reasonable kernel parameterization, or even different parameterizations, to explore sensitivity and different assumptions can be used.

### 4.2. Disaggregating GCM Projections

It is well known that general circulation models (GCMs) present substantial issues in the representation of precipitation, such as overestimation of light rainfall, and underestimation of extreme precipitation (Stephens et al., 2010; Trenberth et al., 2003; Wilcox & Donner, 2007). These problems still persist today (see, e.g., Gehne et al., 2016; Herold et al., 2016; Langousis et al., 2016; Liersch et al., 2016; Svoboda et al., 2017) and even amplify as the resolution of the new generation of models increases (Trenberth et al., 2017). Since monthly GCM simulations are more reliable that daily (e.g., Chun et al., 2014), a common approach is to disaggregate the monthly, or even annual, time series to (sub) daily scales.

Here we use the CPC unified gauge-based analysis of global daily precipitation data set (Xie et al., 2010), which is a gridded data set that has been utilized in numerous evaluation studies of remote sensing, reanalysis, and GCM data products (e.g., DeAngelis et al., 2013; Gehne et al., 2016; Sheffield et al., 2013; Yong et al., 2015). The CPC data set comprises approximately 17,000 stations covering the area defined from 89.75°N to 89.75°S and from 0.25°E to 359.75°E in 0.5° × 0.5° spatial resolution, and for the 1 January 1948 to 31 December 2006 period. The observed daily precipitation time series (Figure 11b) used here is from a 0.5° × 0.5° square region (41.0–41.5°N and 238.5–239.0°E) aggregated to the monthly scale for the sake of comparison (Figure 11b). We also used the BCSD-CMIP5-Climate-monthly data product from the Downscaled CMIP3 and CMIP5 Hydrology Projections Version 3.0 (Reclamation, 2014; https://gdo-dcp.ucllnl.org/downscaled_cmip_projections/). The data used are downscaled in space by the data provider using the "*Bias-Correction and Spatial Disaggregation (BCSD) technique*" (Reclamation, 2013; Wood et al., 2002; Wood et al., 2004). Specifically, we use three GCM simulations of the CMIP5, that is, the monthly precipitation estimates under the rcp8.5 emission scenario from the CNRM-CM5 (Figure 11c), GISS-E2-R, and IPSL-CM5B-LR models at a 0.625° × 0.625° grid for the period 1950–2100 CE. Note that the rcp8.5 refer to future projections from 2006 to 2100 and do not include the period 1950–2005. The time series used here (e.g., Figure 11c) were the merged data product of both historical and future simulations (downloaded from http://iridl.ldeo.columbia.edu).

Following the method described in section 2, we estimate, on a monthly basis, the probability of dry days $p_0$ and we fit the Generalized Gamma ($\mathcal{GG}$) distribution to the observed nonzero daily precipitation using the

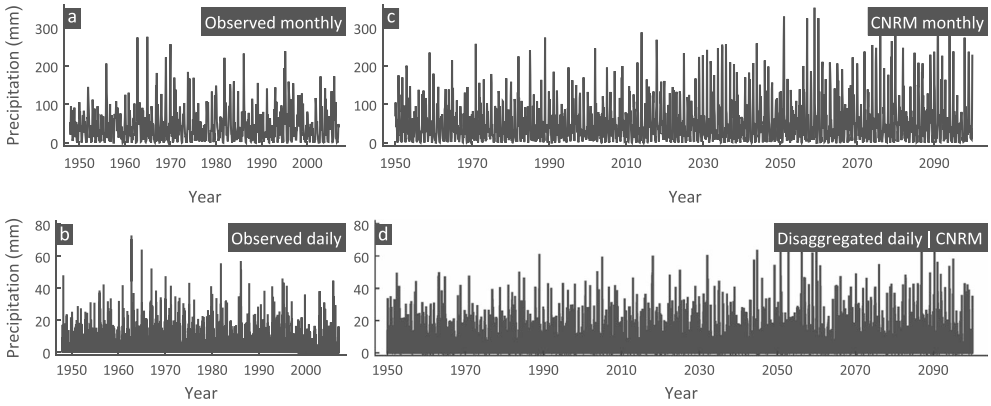


**Figure 11.** (a) Observed monthly and (b) observed daily precipitation over a 0.5° × 0.5° grid in California; (c) monthly projection time series (including the historical 1950–2005 period) from a GCM model (CNRM-CM5); (d) daily time series by disaggregating the monthly CNRM projection.

method of L-moments (see Figure S5) assuming that the process is stationary. Subsequently, we use the Weibull parametric ACS, given by

$$\rho_W(\tau; b, c) = \exp\left(-\left(\frac{\tau}{b}\right)^c\right) \tag{15}$$

with $b > 0$ and $c > 0$, to describe the empirical autocorrelation of daily precipitation and we estimate the parent-Gaussian ACS (Figure S6) of each month, which can be reproduced with sufficient accuracy by an AR($p$) of order $p = 7$ days. The disaggregation scheme was finally applied to the three monthly GCM projections. Comparing Figures 11b and 11d highlights the similarity between the daily disaggregated time series of the CRNM model and the observed daily series.

Of course, a more detailed comparison (see Figure S7) of the empirical distributions of nonzero disaggregated daily precipitation from the three GCM monthly projections with the target $\mathcal{GG}$ distribution reveals some differences for some months, yet this is exactly what we expect, and actually what we desire, as monthly GCM projections differ statistically from the observed monthly precipitation, and thus, the disaggregation scheme (as demonstrated in section 4) has to adapt. In any case, we stress the realistic results, which are also apparent when comparing the empirical ACSs of the disaggregated daily precipitation from three GCM monthly projections with target Weibull ACS assessed from the observed data (see Figure S8).

Similarly, a straightforward comparison of basic statistics (Figure 12), that is, probability of dry days, mean daily precipitation, second L-moment, and L-skewness between the observed daily time series versus the daily disaggregated, clearly shows their similarity, yet in some months differences are apparent. Of course, we stress again that if the GCM projections are nonstationary, then this should be reflected also at the fine-scale process, and thus statistics shown in Figure 12 (or the box plots in Figure 13) express an average state. For example, the daily mean value of December for the CNRM projection (≅6 mm) is almost 50% higher than the observed (≅4 mm), or, higher L-skewness (usually implying more extremes) is observed for August for the GISS projection. Finally, an side-by-side comparison among monthly (Figure 12a) and among daily values (Figure 12b) in terms of box plots (Figure 13, whiskers, indicate the 90% range of values) shows a "transfer" of the difference among the monthly values to daily disaggregated values. For example, the pattern of rank-based indices such as medians or the interquartile range (as expression of variance) at the monthly scale is also "transferred" at the daily scale for almost all months. Yet it is interesting to note how this pattern is smoothed in many months due to contrasting effects. In fact, the disaggregation kernel drives the statistics toward the observed ones, while the constraints force the scheme to adapt in order to replicate the monthly differences.

Ideally, a climate model has to adequately simulate the process of interest at the timescale of interest (a complete discussion on statistical downscaling and bias correction in climate research can be found in Maraun and Widmann, 2018). Yet as climate models are still not able to resolve important fine-scale features,

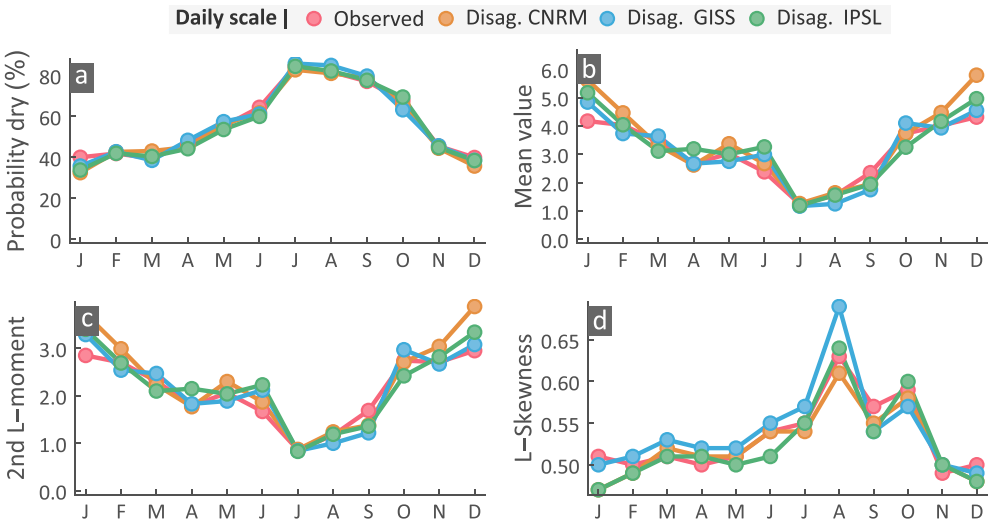


**Figure 12.** Observed daily time series (Figure 11b) versus daily disaggregated from three monthly GCM projections. Comparison of (a) probability dry, (b) mean value, (c) second L-moment, and (d) L-skewness.

disaggregation methods still offer a valuable alternative. As a general comment we stress that disaggregating climate model projections is by necessity based on specific assumptions about the processes at the fine scale. Clearly, any statistical parameter of the disaggregation model could be time variant or nonstationary introducing a large degree of complexity and uncertainty. There is evidence, for example, that the space-time structure of mesoscale convective systems will be changing in the future (e.g., Lenderink & van Meijgaard, 2008; Westra, Alexander et al., 2012) altering not only marginal statistics but also intricate temporal dynamics. This imposes demands on the disaggregation models as to the imposed complexity of the nonstationary marginal and ACS. Here we do not claim that disaggregating a monthly GCM projection, for example, to hourly, results in a process that encapsulates precisely the future hourly characteristics. Rather, we show that it is technically feasible to disaggregate a projection based on the precise statistical properties of the past, or, as we show in the next section, to disaggregated by assuming general nonstationary scenarios.

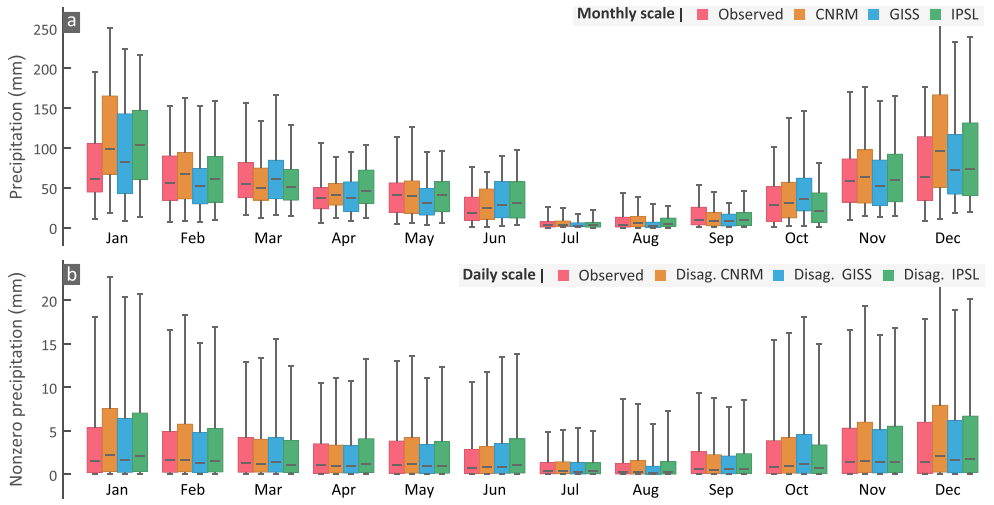


**Figure 13.** Box plots (whiskers indicate the 90% range of values) comparing (a) the observed monthly precipitation over a grid box in California with the projections of three GCM models, and (b) the observed with the disaggregated daily precipitation of the three monthly GCM projections.

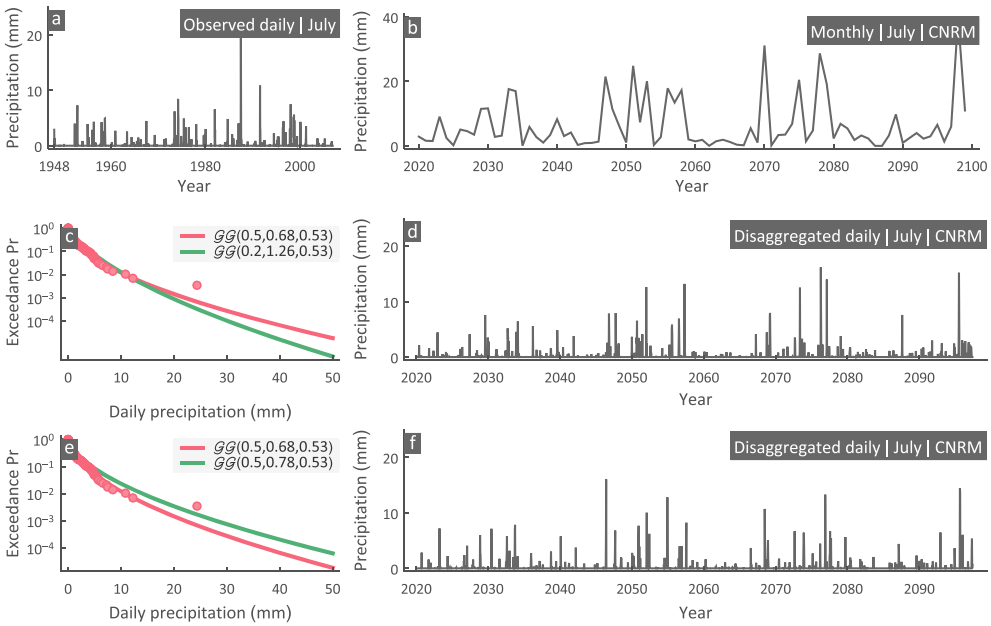


**Figure 14.** Disaggregation of monthly projected precipitation to daily based on the explicit nonstationary framework. (a) Observed daily precipitation for July. (b) Projected monthly. (c) Starting (red) and ending (green) marginal distributions of the disaggregation kernels, over the simulation period (2020–2099), expressing a 40% linear increase in the mean value of nonzero precipitation (Scenario 1); red dots show the empirical distribution of the historical data. (d) Disaggregated daily time series based on Scenario 1. (e and f) Similar to (c) and (d) assuming 40% linear increase in the mean value and 30% in the standard deviation (Scenario 2).

### 4.3. Explicit Nonstationary Disaggregation

We demonstrate the generality and the flexibility of the proposed nonstationary framework by disaggregating the monthly precipitation of the CNRM projection (Figure 11c) using only the projected July values from 2020 to 2099 (80 years; see Figure 14b). Clearly, this framework can be applied likewise for the other months too. We stress that the purpose of this demonstration is to show that it is feasible to disaggregate based on general explicit nonstationary scenarios and not to assess future changes as this is out of the scope of this study. Particularly, based on the empirical (past) daily values of July (Figure 14a), we estimate (using the method of moments) the parameters of the $\mathcal{GG}$ distribution for the nonzero precipitation, that is, $\beta$ = 0.5, $\gamma_1$ = 0.68, and $\gamma_2$ = 0.53 (Figure 14c, red line); the ACS (Figure S6); and the probability dry value $p_0$ = 0.84. Note that the fitted $\mathcal{GG}$ distribution has mean value $\mu_{\mathcal{GG}} = 1.24$ mm and standard deviation $\sigma_{\mathcal{GG}} = 2.25$ mm matching of course the sample statistics of the observed nonzero values. Now let us assume (Scenario 1) that the mean value of the nonzero daily precipitation will increase linearly by 40% by the end of 2099, that is, from 1.24 to 1.74 mm, while the standard deviation, the ACS, the probability dry, and the parameter $\gamma_2$ that controls the behavior of the extremes will remain the same. Of course, this change in the statistical characteristics (mean in this case) is reflected in the parameters of the distribution; that is, we need a new parameter set to express the distribution of the nonzero daily precipitation for every year, which, however, can be easily estimated since the statistics are a priori known. For example, the initial parameters expressing the distribution of the past nonzero daily precipitation at the end of the projection in 2099 become $\beta$ = 0.2, $\gamma_1$ = 1.26, and $\gamma_2$ = 0.53 (Figure 14c, green line); essentially, over this 80-year period we have a progressive transition from the $\mathcal{GG}$ distribution shown in red to the $\mathcal{GG}$ distribution shown in green (Figure 14c). A realization of a daily time series disaggregating the monthly totals in Figure 14b and incorporating this nonstationary scheme is shown in Figure 14d.

Clearly, we can implement any nonstationary scenario and acquire changes not only in the mean but in any other summary statistic, such as the standard deviation, skewness, or L-moments. Similarly, nonstationary scenarios can be implemented by assuming explicit changes in the marginal distribution's parameters; for

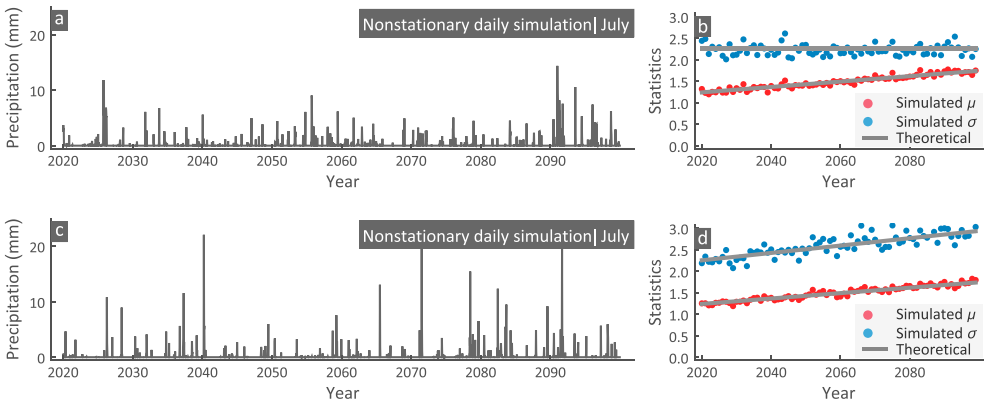


**Figure 15.** Nonstationary simulation of daily precipitation for July (see Figure 14a). (a) Generated time series based on 40% linear increase in the mean by 2099 (Scenario 1), (b) verification of the Scenario 1 model from 1000 simulations, (c) generated time series based on 40% linear increase in the mean and 30% in standard deviation by 2099 (Scenario 2), (d) verification of the Scenario 2 model from 1000 simulations.

example, we may wish to explore an increase in the heaviness of the distribution's tail, which will result in more extremes for the future. Note also that there is no limitation on the function we can choose to express trends; for example, it could be linear or any concave or convex function. For example, let us assume another case (Scenario 2) where in addition to the 40% increase in the mean (over the 80 years) there is also a linear increase in the standard deviation by 30%; that is, by the end of 2099 the standard deviation is expected to increase from 2.25 to 2.96 mm. In terms of the marginal distribution this implies a progressive shift from the $\mathcal{GG}$ distribution depicted in red to the $\mathcal{GG}$ shown in green (see Figure 14e). A corresponding realization of the disaggregation process according to this nonstationary scenario is shown in Figure 14f.

An important aspect we need to stress is the difference between the theoretical statistical properties of the disaggregation kernel and those of the generated blocks. These properties differ as the generated block is constrained to match a specific total at a coarser scale. To clarify by example, on July 2020, the monthly total is 2.87 mm, and the disaggregation kernel (generating the daily values) uses a mixed-type marginal ($p_0 = 0.84$ and nonzero values described by the $\mathcal{GG}(0.5, 0.68, 0.53)$), which has theoretical mean $(1 - p_0)\mu_{\mathcal{GG}} = 0.20$ mm, or else, the theoretical expected monthly total is 31 × 0.20 = 6.20 mm. Yet the optimization procedure forces the selected daily block to match a monthly total of 2.87 mm. This implies that the disaggregated time series cannot be used to verify that indeed the kernels are nonstationary; for example, the theoretical increase in the mean, used in the previous scenarios, will not be reflected in their monthly totals as the monthly totals are specific values that do not coincide with the theoretical expected total of the kernels, which increases every year. However, the nonstationary framework, apart from being mathematically consistent, can be practically verified by simply dropping the disaggregation constrain. Particularly, if we generate a large number (e.g., 1,000) of daily blocks from a nonstationary scenario (Figure 15a shows a single realization from Scenario 1) and isolate the daily values of every year from all realizations and estimate their statistics, we can clearly reveal that the underline process is nonstationary and in agreement with the desired scenario. This is depicted in Figure 15b, which verifies the 40% increase in the mean and the constant value of the standard deviation (Scenario 1). Likewise, Figure 15c shows a single realization from Scenario 2 and Figure 15d verifies that the model generates a 40% increase in the mean and 30% increase in the standard deviation over an 80-year period. For both scenarios, of course, we have verified that the rest of the statistical properties are for every year the desired ones, that is, $p_0 = 0.84$ and $\gamma_2 = 0.53$.

Finally, we note that although the proposed method makes an explicit nonstationary modeling and disaggregation scheme technically feasible, its use should be ideally supported either by physical arguments (e.g., forcing emissions or temperature increases that are expected to cause a known evolution in the precipitation at fine scales) or by deterministic factors that are well identified and introduce nonstationarities in related processes (e.g., land use changes or increasing groundwater withdrawals modifying streamflow). As aforementioned, special care should be taken when nonstationarity is assumed based on trends or fluctuations

resulting from fitting procedures on data. Of course the framework is "by definition" justified, for example, in sensitivity analysis or in exploring arbitrary nonstationary scenarios. For example, we may wish to investigate how a hydrological model reacts when fed with hourly precipitation that evolves in a specific way.

## 5. Concluding Remarks

The problem of producing fine-scale precipitation time series (or of any other hydroclimatic variable) consistent with larger scale observations or model outputs while respecting known, albeit often limited, statistics at the finer scale is termed disaggregation. Disaggregation is essential for practical applications bridging the gap between the observational or climate modeling scales and the scales needed for impact assessment studies, planning, and infrastructure design (e.g., based on the so-called intensity-duration-frequency curves) and risk analysis.

Despite substantial advances, existing disaggregation models exhibit shortcomings as at best they target to preserve a limited and insufficient number of statistics, for example, the first three moments and linear correlations up to only the first few lags, risking underestimation of the distribution's tail, and thus, the behavior of extremes. This stems from the nonunique mapping of a few statistical moments to the full form of a marginal distribution apart from a limited number of parametric distributions, such as normal or lognormal, which do not cover the full range of hydroclimatic variables of interest. Another shortcoming is the lack of generalized methods that can accommodate time-varying statistics, that is, nonstationarity.

Here we present a precise and general disaggregation scheme, called DiPMaC that allows disaggregating a coarse-scale time series into any finer temporal scale. The DiPMaC reproduces (a) the actual probability distribution and linear correlation structure at the fine scale, under stationarity, and arbitrary nonstationary scenarios, and (b) the coarse-scale values. Regarding nonstationarity, we explored two approaches: the first, which is simpler, uses stationary disaggregation kernels, and nonstationarity in the fine-scale process is introduced by forcing the fine-scale stationary process to adapt to a nonstationary coarse-scale process. In the second, which offers more flexibility, the nonstationary properties of the fine-scale process are defined a priori. Moreover, we show how we can optimize the efficiency of the disaggregation procedure using a Bernoulli-trials framework. In this direction, we introduced also an analytical method to evaluate the error caused by the rescaling adjustments (necessary if one wishes the fine scale time series to add up exactly to the coarse-scale series), which allows us to preselect the level of the approximation error in balancing the preservation of the target distribution at the fine scales and the coarse-scale amounts.

Finally, through a number of case studies, we demonstrate the performance and robustness of the DiPMaC algorithm in disaggregating monthly precipitation to hourly, and monthly GCM precipitation projections to daily. We show that DiPMaC meets both objectives of disaggregation methods; that is, it reproduces exactly the target marginal distribution and the ACS at fine scales, as well as, it allows to disaggregate coarse time series based on general nonstationary scenarios. As a future direction, the proposed framework offers the basis for a generalized approach for precise space-time disaggregation across different spatio-temporal scales.

**Acknowledgments**
We thank the three reviewers and the Associate Editor for providing meticulous reviews, which helped us to significantly improve the initial manuscript. This study was partially supported by National Science Foundation (NSF) grants (NSF WSC: EAR-1209402, NSF LIFE: EAR-1242458, and NSF CMMI-1635797), National Aeronautics and Space Administration (NASA) grant (NNX16AO56G), National Oceanic and Atmospheric Administration (NOAA) grant (NA14OAR4310222), and California Energy Commission grant (500-15-005). The data used in this study are freely available at https://www.ncdc.noaa.gov/ and https://cmip.llnl.gov/cmip5/data_portal.html.

## References

Beersma, J. J., & Buishand, T. A. (2003). Multi-site simulation of daily precipitation and temperature conditional on the atmospheric circulation. *Climate Research*, *25*(2), 121–133. https://doi.org/10.3354/cr025121

Box, G. E., & Cox, D. R. (1964). An analysis of transformations. *Journal of the Royal Statistical Society: Series B: Methodological*, *26*(2), 211–252.

Cheng, L., & AghaKouchak, A. (2014). Nonstationary precipitation intensity-duration-frequency curves for infrastructure design in a changing climate. *Scientific Reports*, *4*(1), 7093. https://doi.org/10.1038/srep07093

Cheng, L., AghaKouchak, A., Gilleland, E., & Katz, R. W. (2014). Non-stationary extreme value analysis in a changing climate. *Climatic Change*, *127*(2), 353–369. https://doi.org/10.1007/s10584-014-1254-5

Chun, K. P., Wheater, H. S., & Barr, A. G. (2014). A multivariate comparison of the BERMS flux-tower climate observations and Canadian Coupled Global Climate Model (CGCM3) outputs. *Journal of Hydrology*, *519*, 1537–1550. https://doi.org/10.1016/j.jhydrol.2014.08.059

Connolly, R. D., Schirmer, J., & Dunn, P. K. (1998). A daily rainfall disaggregation model. *Agricultural and Forest Meteorology*, *92*(2), 105–117. https://doi.org/10.1016/S0168-1923(98)00088-4

Cowpertwait, P. S. P., O'Connell, P. E., Metcalfe, A. V., & Mawdsley, J. A. (1996). Stochastic point process modelling of rainfall. II. Regionalisation and disaggregation. *Journal of Hydrology*, *175*(1–4), 47–65.

DeAngelis, A. M., Broccoli, A. J., & Decker, S. G. (2013). A comparison of CMIP3 simulations of precipitation over North America with observations: Daily statistics and circulation features accompanying extreme events. *Journal of Climate*, *26*(10), 3209–3230. https://doi.org/10.1175/JCLI-D-12-00374.1

Deidda, R. (2000). Rainfall downscaling in a space-time multifractal framework. *Water Resources Research*, *36*(7), 1779–1794. https://doi.org/10.1029/2000WR900038

Dobson, A. J., & Barnett, A. (2008). *An introduction to generalized linear models* (3rd ed.). Boca Raton, FL: CRC Press.

Gehne, M., Hamill, T. M., Kiladis, G. N., & Trenberth, K. E. (2016). Comparison of global precipitation estimates across a range of temporal and spatial scales. *Journal of Climate*, *29*(21), 7773–7795. https://doi.org/10.1175/JCLI-D-15-0618.1

Giorgi, F., & Mearns, L. O. (1991). Approaches to the simulation of regional climate change: A review. *Reviews of Geophysics*, *29*(2), 191–216. https://doi.org/10.1029/90RG02636

Glasbey, C. A., Cooper, G., & McGechan, M. B. (1995). Disaggregation of daily rainfall by conditional simulation from a point-process model. *Journal of Hydrology*, *165*(1-4), 1–4), 1–9. https://doi.org/10.1016/0022-1694(94)02598-6

Grygier, J. C., & Stedinger, J. R. (1988). Condensed disaggregation procedures and conservation corrections for stochastic hydrology. *Water Resources Research*, *24*(10), 1574–1584. https://doi.org/10.1029/WR024i010p01574

Gupta, V. K., & Waymire, E. (1990). Multiscaling properties of spatial rainfall and river flow distributions. *Journal of Geophysical Research*, *95*(D3), 1999–2009. https://doi.org/10.1029/JD095iD03p01999

Hammer, G. R., & Steurer, P. M. (1997). Data set documentation for hourly precipitation data. *NOAA/NCDC TD3240 Documentation Series, Asheville, NC*, *18*.

Harms, A. A., & Campbell, T. H. (1967). An extension to the Thomas-Fiering model for the sequential generation of streamflow. *Water Resources Research*, *3*(3), 653–661. https://doi.org/10.1029/WR003i003p00653

Hay, L. E., McCabe, G. J., Wolock, D. M., & Ayers, M. A. (1991). Simulation of precipitation by weather type analysis. *Water Resources Research*, *27*(4), 493–501. https://doi.org/10.1029/90WR02650

Herold, N., Alexander, L. V., Donat, M. G., Contractor, S., & Becker, A. (2016). How much does it rain over land? *Geophysical Research Letters*, *43*, 341–348. https://doi.org/10.1002/2015GL066615

Hershenhorn, J., & Woolhiser, D. A. (1987). Disaggregation of daily rainfall. *Journal of Hydrology*, *95*(3–4), 299–322. https://doi.org/10.1016/0022-1694(87)90008-4

Hoshi, K., & Burges, S. J. (1979). Disaggregation of streamflow volumes. *Journal of the Hydraulics Division*, *105*(1), 27–41.

Hosking, J. R. M. (1990). L-moments: Analysis and estimation of distributions using linear combinations of order statistics. *Journal of the Royal Statistical Society: Series B: Methodological*, *52*(1), 105–124.

Hostetler, S. W. (1994). Hydrologic and atmospheric models: The (continuing) problem of discordant scales. *Climatic Change*, *27*(4), 345–350. https://doi.org/10.1007/BF01096266

Karl, T. R., Wang, W.-C., Schlesinger, M. E., Knight, R. W., & Portman, D. (1990). A method of relating general circulation model simulated climate to the observed local climate. Part I: Seasonal statistics. *Journal of Climate*, *3*(10), 1053–1079. https://doi.org/10.1175/1520-0442(1990)003<1053:AMORGC>2.0.CO;2

Kendall, M., & Stuart, A. (1979). *Handbook of statistics*. London: Griffin & Company.

Kim, J. W., Chang, J. T., Baker, N. L., Wilks, D. S., & Gates, W. L. (1984). The statistical problem of climate inversion: Determination of the relationship between local and large-scale climate. *Monthly Weather Review*, *112*(10), 2069–2077. https://doi.org/10.1175/1520-0493(1984)112<2069:TSPOCI>2.0.CO;2

Kossieris, P., Makropoulos, C., Onof, C., & Koutsoyiannis, D. (2018). A rainfall disaggregation scheme for sub-hourly time scales: Coupling a Bartlett-Lewis based model with adjusting procedures. *Journal of Hydrology*, *556*, 980–992. https://doi.org/10.1016/j.jhydrol.2016.07.015

Kottegoda, N. T., Natale, L., & Raiteri, E. (2003). A parsimonious approach to stochastic multisite modelling and disaggregation of daily rainfall. *Journal of Hydrology*, *274*(1-4), 47–61. https://doi.org/10.1016/S0022-1694(02)00356-6

Koutsoyiannis, D., & Onof, C. (2001). Rainfall disaggregation using adjusting procedures on a Poisson cluster model. *Journal of Hydrology*, *246*(1-4), 109–122. https://doi.org/10.1016/S0022-1694(01)00363-8

Kundzewicz, Z. W., & Stakhiv, E. Z. (2010). Are climate models "ready for prime time" in water resources management applications, or is more research needed? *Hydrological Sciences Journal*, *55*(7), 1085–1089. https://doi.org/10.1080/02626667.2010.513211

Lall, U., & Sharma, A. (1996). A nearest neighbor bootstrap for resampling hydrologic time series. *Water Resources Research*, *32*(3), 679–693. https://doi.org/10.1029/95WR02966

Lane, W. L. (1979). *Applied stochastic techniques (LAST last computer package): User manual, division of planning technical services*. Denver: USBR.

Lane, W. L., & Frevert, D. K. (1988). Applied stochastic techniques: LAST computer package: user manual.

Langousis, A., Mamalakis, A., Deidda, R., & Marrocu, M. (2016). Assessing the relative effectiveness of statistical downscaling and distribution mapping in reproducing rainfall statistics based on climate model results. *Water Resources Research*, *52*, 471–494. https://doi.org/10.1002/2015WR017556

Lenderink, G., & van Meijgaard, E. (2008). Increase in hourly precipitation extremes beyond expectations from temperature changes. *Nature Geoscience*, *1*(8), 511–514. https://doi.org/10.1038/ngeo262

Liersch, S., Tecklenburg, J., Rust, H., Dobler, A., Fischer, M., Kruschke, T., et al. (2016). Are we using the right fuel to drive hydrological models? A climate impact study in the Upper Blue Nile. *Hydrology and Earth System Sciences Discussions*, 1–34. https://doi.org/10.5194/hess-2016-422

Lins, H. F., & Cohn, T. A. (2011). Stationarity: Wanted dead or alive? *JAWRA Journal of the American Water Resources Association*, *47*(3), 475–480. https://doi.org/10.1111/j.1752-1688.2011.00542.x

Lombardo, F., Volpi, E., & Koutsoyiannis, D. (2012). Rainfall downscaling in time: Theoretical and empirical comparison between multifractal and Hurst-Kolmogorov discrete random cascades. *Hydrological Sciences Journal*, *57*(6), 1052–1066. https://doi.org/10.1080/02626667.2012.695872

Lombardo, F., Volpi, E., Koutsoyiannis, D., & Papalexiou, S. M. (2014). Just two moments! A cautionary note against use of high-order moments in multifractal models in hydrology. *Hydrology and Earth System Sciences*, *18*(1), 243–255. https://doi.org/10.5194/hess-18-243-2014

Lombardo, F., Volpi, E., Koutsoyiannis, D., & Serinaldi, F. (2017). A theoretically consistent stochastic cascade for temporal disaggregation of intermittent rainfall. *Water Resources Research*, *53*, 4586–4605. https://doi.org/10.1002/2017WR020529

Loucks, D. P., Stedinger, J. R., & Haith, D. A. (1981). *Water resource systems planning and analysis*. Englewood Cliffs, NJ: Prentice-Hall.

Lovejoy, S., & Schertzer, D. (1990). Multifractals, universality classes and satellite and radar measurements of cloud and rain fields. *Journal of Geophysical Research*, *95*(D3), 2021–2034. https://doi.org/10.1029/JD095iD03p02021

Lu, Y., & Qin, X. S. (2014). Multisite rainfall downscaling and disaggregation in a tropical urban area. *Journal of Hydrology*, *509*, 55–65. https://doi.org/10.1016/j.jhydrol.2013.11.027

Maraun, D. (2013). Bias correction, quantile mapping, and downscaling: Revisiting the inflation issue. *Journal of Climate*, *26*(6), 2137–2143. https://doi.org/10.1175/JCLI-D-12-00821.1

Maraun, D., Wetterhall, F., Ireson, A. M., Chandler, R. E., Kendon, E. J., Widmann, M., et al. (2010). Precipitation downscaling under climate change: Recent developments to bridge the gap between dynamical models and the end user. *Reviews of Geophysics*, *48*, RG3003. https://doi.org/10.1029/2009RG000314

Maraun, D., & Widmann, M. (2018). *Statistical downscaling and bias correction for climate research*. Cambridge: Cambridge University Press. https://doi.org/10.1017/9781107588783

Matalas, N. C. (1967). Mathematical assessment of synthetic hydrology. *Water Resources Research*, *3*(4), 937–945. https://doi.org/10.1029/WR003i004p00937

Mejia, J. M., & Rousselle, J. (1976). Disaggregation models in hydrology revisited. *Water Resources Research*, *12*(2), 185–186. https://doi.org/10.1029/WR012i002p00185

Molnar, P., & Burlando, P. (2005). Preservation of rainfall properties in stochastic disaggregation by a simple random cascade model. *Atmospheric Research*, *77*(1-4), 137–151. https://doi.org/10.1016/j.atmosres.2004.10.024

Nowak, K., Prairie, J., Rajagopalan, B., & Lall, U. (2010). A nonparametric stochastic approach for multisite disaggregation of annual to daily streamflow. *Water Resources Research*, *46*, W08529. https://doi.org/10.1029/2009WR008530

Obeysekera, J., & Salas, J. D. (2016). Frequency of recurrent extremes under nonstationarity. *Journal of Hydrologic Engineering*, *21*(5), 04016005. https://doi.org/10.1061/(ASCE)HE.1943-5584.0001339

Oliveira, G. C., Kelman, J., Pereira, M. V. F., & Stedinger, J. R. (1988). A representation of spatial cross correlations in large stochastic seasonal streamflow models. *Water Resources Research*, *24*(5), 781–785. https://doi.org/10.1029/WR024i005p00781

Olsson, J. (1998). Evaluation of a scaling cascade model for temporal rain-fall disaggregation. *Hydrology and Earth System Sciences Discussions*, *2*(1), 19–30. https://doi.org/10.5194/hess-2-19-1998

Papalexiou, S. M. (2018). Unified theory for stochastic modelling of hydroclimatic processes: Preserving marginal distributions, correlation structures, and intermittency. *Advances in Water Resources*, *115*, 234–252. https://doi.org/10.1016/j.advwatres.2018.02.013

Papalexiou, S. M., AghaKouchak, A., & Foufoula-Georgiou, E. (2018). A diagnostic framework for understanding climatology of tails of hourly precipitation extremes in the United States. *Water Resources Research*, *54*. https://doi.org/10.1029/2018WR022732

Papalexiou, S. M., & Koutsoyiannis, D. (2012). Entropy based derivation of probability distributions: A case study to daily rainfall. *Advances in Water Resources*, *45*, 51–57. https://doi.org/10.1016/j.advwatres.2011.11.007

Papalexiou, S. M., & Koutsoyiannis, D. (2016). A global survey on the seasonal variation of the marginal distribution of daily precipitation. *Advances in Water Resources*, *94*, 131–145. https://doi.org/10.1016/j.advwatres.2016.05.005

Peel, M. C., Wang, Q., Vogel, R. M., & McMahon, T. A. (2001). The utility of L-moment ratio diagrams for selecting a regional probability distribution. *Hydrological Sciences Journal*, *46*(1), 147–155. https://doi.org/10.1080/02626660109492806

Pereira, M. V. F., Oliveira, G. C., Costa, C. C. G., & Kelman, J. (1984). Stochastic streamflow models for hydroelectric systems. *Water Resources Research*, *20*(3), 379–390. https://doi.org/10.1029/WR020i003p00379

Perica, S., & Foufoula-Georgiou, E. (1996). Model for multiscale disaggregation of spatial rainfall based on coupling meteorological and scaling. *Journal of Geophysical Research*, *101*, 26–347.

Portela, M. M., & Silva, A. T. (2016). Disaggregation modelling of annual flows into daily streamflows using a new approach of the method of fragments. *Water Resources Management*, *30*(15), 5589–5607. https://doi.org/10.1007/s11269-016-1402-y

Prairie, J., Rajagopalan, B., Lall, U., & Fulp, T. (2007). A stochastic nonparametric technique for space-time disaggregation of streamflows. *Water Resources Research*, *43*, W03432. https://doi.org/10.1029/2005WR004721

Pui, A., Sharma, A., Mehrotra, R., Sivakumar, B., & Jeremiah, E. (2012). A comparison of alternatives for daily to sub-daily rainfall disaggregation. *Journal of Hydrology*, *470*, 138–157.

Ragno, E., AghaKouchak, A., Love, C. A., Cheng, L., Vahedifard, F., & Lima, C. H. R. (2018). Quantifying changes in future intensity-duration-frequency curves using multimodel ensemble simulations. *Water Resources Research*, *54*, 1751–1764. https://doi.org/10.1002/2017WR021975

Read, L. K., & Vogel, R. M. (2016). Hazard function analysis for flood planning under nonstationarity. *Water Resources Research*, *52*, 4116–4131. https://doi.org/10.1002/2015WR018370

Reclamation (2013). *Downscaled CMIP3 and CMIP5 climate and hydrology projections: Release of downscaled CMIP5 climate projections, comparison with preceding information, and summary of user needs* (p. 104). U.S. Department of the Interior, Bureau of Reclamation, Technical Service Center, Denver, CO.

Reclamation (2014). *Downscaled CMIP3 and CMIP5 climate and hydrology projections: Release of downscaled CMIP5 climate projections, comparison with preceding information, and summary of user needs* (p. 110). U.S. Department of the Interior, Bureau of Reclamation, Technical Service Center, Denver, Colorado.

Rodriguez-Iturbe, I., Cox, D. R., & Isham, V. (1987). Some models for rainfall based on stochastic point processes. *Proceedings of the Royal Society of London A: Mathematical, Physical and Engineering Sciences*, *410*(1839), 269–288. https://doi.org/10.1098/rspa.1987.0039

Salas, J. D. (1980). *Applied modeling of hydrologic time series*. Littleton, CO: Water Resources Publication.

Salas, J. D., Tabios, G. Q., & Bartolini, P. (1985). Approaches to multivariate modeling of water resources time series. *JAWRA Journal of the American Water Resources Association*, *21*(4), 683–708. https://doi.org/10.1111/j.1752-1688.1985.tb05383.x

Serinaldi, F. (2010). Multifractality, imperfect scaling and hydrological properties of rainfall time series simulated by continuous universal multifractal and discrete random cascade models. *Nonlinear Processes in Geophysics*, *17*(6), 697–714. https://doi.org/10.5194/npg-17-697-2010

Serinaldi, F., Kilsby, C. G., & Lombardo, F. (2018). Untenable nonstationarity: An assessment of the fitness for purpose of trend tests in hydrology. *Advances in Water Resources*, *111*, 132–155. https://doi.org/10.1016/j.advwatres.2017.10.015

Sheffield, J., Camargo, S. J., Fu, R., Hu, Q., Jiang, X., Johnson, N., et al. (2013). North American climate in CMIP5 experiments. Part II: Evaluation of historical simulations of intraseasonal to decadal variability. *Journal of Climate*, *26*(23), 9247–9290. https://doi.org/10.1175/JCLI-D-12-00593.1

Sivakumar, B., Sorooshian, S., Gupta, H. V., & Gao, X. (2001). A chaotic approach to rainfall disaggregation. *Water Resources Research*, *37*(1), 61–72. https://doi.org/10.1029/2000WR900196

Srikanthan, R. (1978). Sequential generation of monthly streamflows. *Journal of Hydrology*, *38*(1–2), 71–80. https://doi.org/10.1016/0022-1694(78)90133-6

Stacy, E. W. (1962). A generalization of the gamma distribution. *The Annals of Mathematical Statistics*, *33*(3), 1187–1192. https://doi.org/10.1214/aoms/1177704481

Stedinger, J. R., Pei, D., & Cohn, T. A. (1985). A condensed disaggregation model for incorporating parameter uncertainty into monthly reservoir simulations. *Water Resources Research*, *21*(5), 665–675. https://doi.org/10.1029/WR021i005p00665

Stedinger, J. R., & Vogel, R. M. (1984). Disaggregation procedures for generating serially correlated flow vectors. *Water Resources Research*, *20*(1), 47–56. https://doi.org/10.1029/WR020i001p00047

Stephens, G. L., L'Ecuyer, T., Forbes, R., Gettelmen, A., Golaz, J.-C., Bodas-Salcedo, A., et al. (2010). Dreary state of precipitation in global models. *Journal of Geophysical Research*, *115*, D24211. https://doi.org/10.1029/2010JD014532

von Storch, H., Zorita, E., & Cubasch, U. (1993). Downscaling of global climate change estimates to regional scales: An application to Iberian rainfall in wintertime. *Journal of Climate*, *6*(6), 1161–1171. https://doi.org/10.1175/1520-0442(1993)006<1161:DOGCCE>2.0.CO;2

Svoboda, V., Hanel, M., Máca, P., & Kyselỳ, J. (2017). Characteristics of rainfall events in regional climate model simulations for the Czech Republic. *Hydrology and Earth System Sciences*, *21*(2), 963–980. https://doi.org/10.5194/hess-21-963-2017

Tao, P. C., & Delleur, J. W. (1976). Multistation, multiyear synthesis of hydrologic time series by disaggregation. *Water Resources Research*, *12*(6), 1303–1312. https://doi.org/10.1029/WR012i006p01303

Todini, E. (1980). The preservation of skewness in linear disaggregation schemes. *Journal of Hydrology*, *47*(3–4), 199–214. https://doi.org/10.1016/0022-1694(80)90093-1

Trenberth, K. E., Dai, A., Rasmussen, R. M., & Parsons, D. B. (2003). The changing character of precipitation. *Bulletin of the American Meteorological Society*, *84*(9), 1205–1218. https://doi.org/10.1175/BAMS-84-9-1205

Trenberth, K. E., Zhang, Y., & Gehne, M. (2017). Intermittency in precipitation: Duration, frequency, intensity, and amounts using hourly data. *Journal of Hydrometeorology*, *18*(5), 1393–1412. https://doi.org/10.1175/JHM-D-16-0263.1

Tripathi, S., Srinivas, V. V., & Nanjundiah, R. S. (2006). Support vector machine approach to downscale precipitation in climate change scenarios. In *World Environmental and Water Resource Congress 2006: Examining the Confluence of Environmental and Water Concerns* (pp. 1–10). Retrieved from https://ascelibrary.org/doi/10.1061/40856%28200%2945

Tsoukalas, I., Papalexiou, S. M., Efstratiadis, A., & Makropoulos, C. (2018). A cautionary note on the reproduction of dependencies through linear stochastic models with non-Gaussian white noise. *Water*, *10*(6), 771. https://doi.org/10.3390/w10060771

Valencia, D. R., & Schaake, J. C. (1972). *A disaggregation model for time series analysis and synthesis*. Rep. 149, Ralph M. Parsons Lab. For Water Resour. and Hydrodyn., Mass. Inst. of Technol., Cambridge.

Valencia, D. R., & Schaake, J. C. (1973). Disaggregation processes in stochastic hydrology. *Water Resources Research*, *9*(3), 580–585. https://doi.org/10.1029/WR009i003p00580

Venugopal, V., Foufoula-Georgiou, E., & Sapozhnikov, V. (1999). A space-time downscaling model for rainfall. *Journal of Geophysical Research*, *104*(D16), 19,705–19,721. https://doi.org/10.1029/1999JD900338

Westra, S., Alexander, L. V., & Zwiers, F. W. (2012). Global increasing trends in annual maximum daily precipitation. *Journal of Climate*, *26*(11), 3904–3918. https://doi.org/10.1175/JCLI-D-12-00502.1

Westra, S., Mehrotra, R., Sharma, A., & Srikanthan, R. (2012). Continuous rainfall simulation: 1. A regionalized subdaily disaggregation approach. *Water Resources Research*, *48*, W01535. https://doi.org/10.1029/2011WR010489

Wigley, T. M. L., Jones, P. D., Briffa, K. R., & Smith, G. (1990). Obtaining sub-grid-scale information from coarse-resolution general circulation model output. *Journal of Geophysical Research*, *95*(D2), 1943–1953. https://doi.org/10.1029/JD095iD02p01943

Wilby, R. L., & Wigley, T. M. L. (1997). Downscaling general circulation model output: A review of methods and limitations. *Progress in Physical Geography*, *21*(4), 530–548. https://doi.org/10.1177/030913339702100403

Wilby, R. L., & Wigley, T. M. L. (2000). Precipitation predictors for downscaling: Observed and general circulation model relationships. *International Journal of Climatology*, *20*(6), 641–661. https://doi.org/10.1002/(SICI)1097-0088(200005)20:6<641::AID-JOC501>3.0.CO;2-1

Wilcox, E. M., & Donner, L. J. (2007). The frequency of extreme rain events in satellite rain-rate estimates and an atmospheric general circulation model. *Journal of Climate*, *20*(1), 53–69. https://doi.org/10.1175/JCLI3987.1

Wood, A. W., Leung, L. R., Sridhar, V., & Lettenmaier, D. P. (2004). Hydrologic implications of dynamical and statistical approaches to downscaling climate model outputs. *Climatic Change*, *62*(1–3), 189–216. https://doi.org/10.1023/B:CLIM.0000013685.99609.9e

Wood, A. W., Maurer, E. P., Kumar, A., & Lettenmaier, D. P. (2002). Long-range experimental hydrologic forecasting for the eastern United States. *Journal of Geophysical Research*, *107*(D20), 4429. https://doi.org/10.1029/2001JD000659

Xie, P., Chen, M., & Shi, W. (2010). CPC unified gauge-based analysis of global daily precipitation. In *Preprints, 24th Conf. on Hydrology, Atlanta, GA, Amer. Meteor. Soc* (Vol. 2).

Xue, Y., Janjic, Z., Dudhia, J., Vasic, R., & De Sales, F. (2014). A review on regional dynamical downscaling in intraseasonal to seasonal simulation/prediction and major factors that affect downscaling ability. *Atmospheric Research*, *147-148*, 68–85. https://doi.org/10.1016/j.atmosres.2014.05.001

Yee, T. W., & Stephenson, A. G. (2007). Vector generalized linear and additive extreme value models. *Extremes*, *10*, 1), 1–1), 19.

Yong, B., Liu, D., Gourley, J. J., Tian, Y., Huffman, G. J., Ren, L., & Hong, Y. (2015). Global view of real-time TRMM multisatellite precipitation analysis: Implications for its successor global precipitation measurement mission. *Bulletin of the American Meteorological Society*, *96*(2), 283–296. https://doi.org/10.1175/BAMS-D-14-00017.1

Zorita, E., & von Storch, H. (1999). The analog method as a simple statistical downscaling technique: Comparison with more complicated methods. *Journal of Climate*, *12*(8), 2474–2489. https://doi.org/10.1175/1520-0442(1999)012<2474:TAMAAS>2.0.CO;2